Draft version September 26, 2009
Preprint typeset using LaTeX style emulateapj v. 08/22/09

HUBBLE SPACE TELESCOPE SURVEY OF INTERSTELLAR HIGH-VELOCITY SI III

Joseph A. Collins[1], J. Michael Shull
University of Colorado, CASA, Department of Astrophysical & Planetary Sciences, Campus Box 389, Boulder, CO 80309
jcollins@casa.colorado.edu, michael.shull@colorado.edu

and

Mark L. Giroux
East Tennessee State University, Department of Physics & Astronomy,
Box 70652, Johnson City, TN 37614, girouxm@etsu.edu
Draft version September 26, 2009

ABSTRACT

We describe an ultraviolet spectroscopic survey of interstellar high-velocity cloud (HVC) absorption in the strong λ1206.500 line of Si III using the Space Telescope Imaging Spectrograph aboard the *Hubble Space Telescope*. Because the Si III line is 4–5 times stronger than O VI λ1031.926, it provides a sensitive probe of ionized gas down to column densities $N_{SiIII} \approx 5 \times 10^{11}$ cm^{-2} at Si III equivalent width 10 mÅ. We detect high-velocity Si III over $91 \pm 4\%$ of the sky (53 of 58 sight lines); 59% of the HVCs show negative LSR velocities. Per sight line, the mean HVC column density is $\langle \log N_{SiIII} \rangle = 13.19 \pm 0.45$, while the mean for all 90 velocity components is 12.92 ± 0.46. Lower limits due to Si III line saturation are included in this average, so the actual mean/median values are even higher. The Si III appears to trace an extensive ionized component of Galactic halo gas at temperatures $10^{4.0-4.5}$ K indicative of a cooling flow. Photoionization models suggest that typical Si III absorbers with $12.5 < \log N_{SiIII} < 13.5$ have total hydrogen column densities $N_H \approx 10^{18}$–10^{19} cm^{-2} for gas of hydrogen density $n_H \approx 0.1$ cm^{-3} and 10% solar metallicity. With typical neutral fractions $N_{HI}/N_H \approx 0.01$, these HVCs may elude even long-duration 21-cm observations at Arecibo, the EVLA, and other radio facilities. However, if Si III is associated with higher density gas, $n_H \geq 1$ cm^{-3}, the corresponding neutral hydrogen could be visible in deep observations. This reservoir of ionized gas may contain 10^8 $M_\odot$ and produce a mass infall rate of 1 $M_\odot$ yr^{-1} to the Galactic disk.

Subject headings: Galaxy: halo — ISM: clouds — ISM: abundances — ultraviolet: general

1. INTRODUCTION

Over the past several decades, radio maps and spectra of H I 21-cm emission have revealed a significant population of objects with velocities incompatible with standard models of Galactic rotation, the so-called high-velocity clouds (Wakker & van Woerden 1997). In the Milky Way, high-velocity clouds (HVCs) and intermediate-velocity clouds (IVCs) are distinguished by their velocities in the local standard of rest (LSR), with a nominal population break at $|V_{LSR}| = 90-100$ km s^{-1}. Following the convention of Wakker & van Woerden (1997), we define IVCs to lie between $|v_{LSR}| \approx 30$–90 km s^{-1} and HVCs to have $|v_{LSR}| > 90$ km s^{-1}.

Far more sensitive probes of HVCs and IVCs have become available through ultraviolet (UV) absorption-line studies of zero-redshift absorption lines in the spectra of background quasars taken with the *Hubble Space Telescope* (*HST*) and the *Far Ultraviolet Spectroscopic Explorer* (*FUSE*). The far ultraviolet offers much greater sensitivity to low column density gas, such as HVC surveys in O VI (Sembach et al. 2003) and Si III (Shull et al. 2009), and they offer the best means for tracing ionized HVC gas. The fractional HVC sky coverage using these lines range from 60 to 90%, reflecting both the higher UV sensitivity and the fact that HVCs contain substantial amounts of ionized gas undetectable in 21-cm emission. Consequently, the total reservoir of HVC gas is considerably larger than seen in H I, and the cooling mass-infall rate could be as high as $1 M_\odot$ yr^{-1} (Shull et al. 2009). This infall provides a significant portion of the replenishment rate required to fuel star formation in the Galactic disk. On the scale of the Galactic halo, the G-dwarf problem (Pagel 1994) has inspired a picture of continuous infall of low-metallicity gas onto the Milky Way disk.

On larger scales, HVCs have been invoked to explain phenomena such as the "missing dwarfs" predicted in simulations of Local Group formation (Blitz et al. 1999) or the potential reservoir of hot baryons located in the circumgalactic medium of large galaxies (Nicastro et al. 2003) or in the true intergalactic medium (IGM). Whatever their distance, HVCs may trace building blocks of the Galaxy or Local Group (Putman et al. 2009). Their study illuminates the processes of local gaseous infall/outflow, structure formation, and chemical enrichment of the Milky Way and IGM. Most of the framework used to interpret emission and absorption from high-velocity gas comes from a thorough understanding of the kinematics, distribution, and composition of the H I column density distribution. At the high end of this distribution are those HVCs mapped through all-sky H I 21-cm emission surveys such as the Leiden-Dwingleoo Survey (LDS; Hartmann & Burton 1997), sensitive to column densities down to $N_{HI} \approx 10^{18.5}$ to 10^{19} cm^{-2} for a standard HVC width of $\Delta V \sim 100$ km s^{-1}. The

[1] Also at Front Range Community College, Larimer Campus, 4616 S. Shields St., Fort Collins, CO 80526

high-velocity H I emission sky is dominated by objects of large angular size known as HVC Complexes. Inferring a scaled mass as a function of distance (e.g., Wakker et al. 1999) restricts the large complexes to the Galactic halo. Uncertain distances to HVCs made it difficult to distinguish between various models and the role of HVCs in Galaxy evolution. However, recent work searching for Ca II absorption in spectra of Galactic halo stars puts the distance to HVC Complex C at 10 ± 2.5 kpc (Thom et al. 2008; Wakker et al. 2007). Distance to other HVCs (Wakker et al. 2008) have been constrained to 5–15 kpc by this technique.

Our group and others have devoted considerable attention to Complex C, which is pierced by 11 QSO sight lines observable with UV spectrographs on *HST* and *FUSE*. Based on O I and S II abundances, its metallicity has been measured at $Z/Z_{\odot} = 0.09 - 0.29$ (Wakker et al. 1999; Gibson et al. 2001; Richter et al. 2001; Tripp et al. 2003; Collins, Shull, & Giroux 2003, 2007, hereafter CSG03 and CSG07). These surveys found that Complex C contains $\sim 10^7$ $M_{\odot}$ of gas, with approximately equal amounts of neutral and ionized components. Some of this HVC is mixing with Galactic gas as it falls toward the disk. At an approximate elevation of 10 kpc and infall velocity of -150 km s^{-1}, the gas in Complex C will fall onto the Galactic disk over the next 50–100 Myr, with an average infall rate of 0.1 $M_{\odot}$ yr^{-1}. Fox et al. (2004) and CSG07 investigated the highly ionized portions of Complex C, reinforcing the notion that the cloud is interacting with the Galactic halo through cooling and dynamic instabilities.

While ever-deeper H I emission studies have pushed the catalog of known HVCs to smaller N_{HI}, the most dramatic strides in our knowledge of the low end of the HVC column density distribution have come from UV spectroscopy. The *FUSE* survey (Sembach et al. 2003, hereafter S03) of O VI detected high-velocity absorption in $60 - 85\%$ of extragalactic sight lines. Our *HST* study in the strong line of Si III (Shull et al. 2009) found HVCs in 30 of 37 sight lines (approximately 80%). Although many of these high-velocity O VI and Si III detections correlate directly with H I-detected HVCs, a significant portion of the population has no corresponding 21-cm detections. The O VI HVCs not detected in H I emission have been termed "highly ionized HVCs" (Sembach et al. 1999). However, our recent studies of this population (Collins, Shull, & Giroux 2004, 2005; hereafter CSG04, CSG05) have detected neutral and low-ionized gas at the same velocities. We suggest that this HVC population is simply an extension of the usual HVC distribution, but with H I column densities below the sensitivity level of current 21-cm emission surveys.

One interpretation (Nicastro et al. 2002; 2003) of the kinematics and ionization properties of the highly ionized HVCs associates these absorbers with warm-hot O VII and O VIII absorbing IGM filaments or WHIM (Cen & Ostriker 1999) in the Local Group. We have argued (CSG04, CSG05) that these HVCs more likely reside in the Galactic halo, based on three major lines of evidence. First, the mass in hot gas would be unreasonably large, $M_{\rm hot} \sim [10^{12} M_{\odot}] d^2_{\rm Mpc}$ (see CSG04), compared to dynamical measures of the Milky Way and Local Group if all the O VI absorbers traced a WHIM filament at Mpc distances in the Local Group. Distributing the HVCs throughout the Local Group only lowers this estimate by factors of 2–3. Second, the kinematics of HVCs are consistent with a combination of infall onto the Galaxy and outflows in other directions In the current sample, as well as that of Shull et al. (2009), about 60% of the HVCs have negative LSR velocities. Third, 10 of the 12 highly-ionized HVCs surveyed in CSG05 contain neutral gas or low ions (C II, Si II, Si III), suggesting that these HVCs have densities $n_H \gg 10^{-4}$ cm^{-3} to avoid being photoionized by metagalactic radiation. We argue therefore that these HVCs are similar in ionization properties to the population observed in 21-cm emission, but with lower neutral hydrogen column densities, log $N_{\rm HI} \leq 18$. The higher ionization states (O VI, C IV, Si III, etc.) seen in these HVCs suggests that they contain multiphase gas, produced by both photoionization and collisional ionization (shocks or interfaces with hotter halo gas). A recent survey (Fox, Savage, & Wakker 2006; hereafter FSW06) found that high-velocity C III is present in $\sim 80\%$ of the highly-ionized HVCs, consistent with a multiphase interpretation of these HVCs and a Galactic origin. This interpretation is also supported by Zech et al. (2008) who analyzed a highly ionized HVC toward the Globular Cluster M5 (7.5 kpc distance). Given the similarities in ionization properties between the highly ionized HVCs and the 21 cm-detected halo HVCs, a more apt term for the highly ionized HVCs may be "low column HVCs".

The full distribution, kinematics, and covering fraction of the low column density HVCs is not well determined. Although H I Lyα and higher Lyman-series resonance lines are the most sensitive diagnostics of low column density gas, the absorption in high-velocity gas is rarely open to analysis in these lines, owing to severe saturation from Galactic H I absorption and confusion with other resonance lines. Considering elemental abundance, ionization, and oscillator strength, the Si III λ1206.50 line is one of the best (strongest) UV resonance lines for discovering high-velocity gas. Although the Si II λ1260.42 and C II λ1334.53 lines are typically just as strong, the S II λ1259.52 and C II* λ1335.70 lines contaminate large portions of their high-velocity profiles. An additional advantage of the Si III line is that it lies in a relatively line-free part of the spectrum, blueward of Lyα, uncontaminated by the intergalactic Lyα forest, and in most cases, by other IGM lines.

A large number of extragalactic AGN/QSO sight lines have been observed with the Space Telescope Imaging Spectrograph (STIS) on *HST*. These STIS archive spectra cover the $\lambda = 1200$ Å region, enabling us to use the Si III line to map the distribution, covering fraction, and kinematics of HVCs down to total hydrogen column densities $N_{\rm H} \approx 10^{17}$ cm^{-2}, and below the detection limits typically available in H I. In this paper, we present a survey of high-velocity interstellar Si III absorption line along 58 extragalactic sight lines, using archival data taken with the *HST*-STIS E140M echelle and G140M gratings. A previous paper (Shull et al. 2009) presented a study of Si II, Si III and Si IV in HVCs and IVCs in the E140M datasets. The survey data and criteria for their selection are presented in Section 2. The analysis of those data, along with line profiles and measurements, is discussed in Section 3. We explore the overall distribution,

kinematics, and ionization of these HVCs in Section 4. Our conclusions are presented in Section 5.

2. SIGHT LINE SELECTION AND SURVEY DATA

The initial pool of data for this study is the entire archive of *HST*-STIS spectra of extragalactic targets that cover the Si III line. Since we aim to measure absorption features of width ~ 100 km s^{-1}, we only use data taken with the E140M echelle or G140M first-order gratings. The E140M mode provides 7 km s^{-1} resolution over a large bandpass, 1150 – 1700 Å, which covers resonance lines of several important ion species. The G140M grating, when set to cover the 1199–1249 Å range, provides higher sensitivity at the cost of smaller bandpass and lower resolution (~ 25 km s^{-1}) compared to the echelle data. In order to improve detectability of low column density absorbers and to match the resolution provided by the G140M data, we binned all E140M data sets to three pixels. Some sight lines contain both E140M and G140M data covering the Si III line. In these cases, we rely on the E140M datasets, since they provide the opportunity to compare a high-velocity feature in multiple absorption lines and facilitate the identification of IGM and other contaminants.

Once we compiled this set of spectra, we narrowed our survey with a few criteria. First, we limited our survey to datasets with sufficient signal to noise to analyze high-velocity features: $(S/N) \geq 3$ at 1200 Å per resolution element (three binned pixels) for the E140M data and per pixel for the G140M data. Although lower quality data may identify high-velocity features, the continuum is often too noisy to properly establish its velocity extent. Second, we eliminated sight lines from the survey in which absorbers at redshifts $z > 0$ significantly contaminate the high-velocity range of the Si III line. Two sight lines dropped from our survey, 3C 249.1 and Mrk 205, deserve mention. High-velocity Si III at negative velocity is most likely present in each sight line, as evidenced by corresponding detections in other absorption lines. However, the HVC feature is contaminated by intergalactic Lyβ (at $z = 0.176$) toward 3C 249.1 and by intergalactic N I λ1200.71 (at $z = 0.0043$) from a strong Lyα absorber toward Mrk 205.

After we applied the selection criteria, our survey consisted of 58 sight lines, of which 33 and 25 are E140M and G140M datasets, respectively. Absolute wavelength scales were obtained by aligning the peak of H I emission features in sight line data from the Effelsberg 100-m telescope (Wakker et al. 2003) or the Leiden-Dwingleoo Survey (LDS; Hartmann & Burton 1997), when available, with corresponding absorption line features in the STIS data. We generally relied on lines of N I (λ1199.55, 1200.22, 1200.71) and S II (λ1250.58, 1253.81, 1259.52) for this comparison. In a few cases, we could not find an absolute wavelength scale, owing to absence of H I data, or in a few G140M datasets when the available comparison features were not clean enough to use.

3. MEASUREMENT OF HIGH-VELOCITY SI III FEATURES

We now discuss our techniques for investigating Si III absorption from HVCs in our sample of 58 sight lines. In order to measure column densities of ion species, we first extracted individual line profiles from the full *HST*-STIS spectra. These profiles were normalized by fitting low-order polynomials to the continuum $\pm$(3–10) Å about the line in question, although in a number of cases spurious features near the line required using a much larger region for continuum measurement. For each sight line, we searched the region $100 < |v| < 500$ km s^{-1} around the Si III line for any possible absorption from an HVC. If candidate HVC features were found, we attempted to determine whether the feature was due to a contaminant line at redshift $0 < z < z_{QSO}$. This process was more easily performed for E140M spectra, where redshifts of any intervening Lyα absorbers can be determined along with possible contamination of the Si III profile from other absorption lines at the same redshifts. Additionally, several of these sight lines have been examined in the literature for intervening lines, which can also be used to assess possible contamination of the Si III line. If contamination from known IGM absorbers can be ruled out, we can then assume that any detected absorption is due to Si III.

Once we have identified high-velocity Si III absorbers, we determined the relevant velocity range by comparing the Si III profile to other absorption lines in which the high velocity component is detected. In some cases, the H I emission profile can be used to identify the velocity range. The most useful lines for the comparison, however, are the strong lines of Si II λ1260.42 and C II λ1334.53, although in many cases the HVCs can also be detected in O I λ1302.17, the N I triplet at 1199–1200 Å, other Si II lines (e.g., 1193.29 Å, 1304.37 Å, 1526.71 Å), and in the more highly ionized doublets of C IV $\lambda\lambda$1548.20, 1550.77 and Si IV $\lambda\lambda$1393.76, 1402.77. Some of the sight lines are shared by the *FUSE* survey of high-velocity O VI (S03), with which high-velocity Si III features can be compared. The presence of a high-velocity feature in multiple absorption lines provides additional confidence that the Si III profile is uncontaminated by higher redshift absorption features. Some G140M datasets cover only 1199–1249 Å, limiting our ability to establish an accurate integration range, confirm detections, and search for higher-redshift contaminants.

Figures 1 and 2 show Si III profiles from E140M and G140M data, respectively, for all 58 sight lines surveyed. Also shown are the velocity extents of each high-velocity component analyzed. Once an integration range is established, we measure the equivalent width, W_λ, of the high-velocity feature. Using the most recent value of oscillator strength for the Si III line ($f = 1.63$; Morton 2003), we measured the column density of high-velocity Si III using the apparent optical depth method (AOD; Savage & Sembach 1991), which applies to lines that are optically thin. The linear relation between Si III equivalent width and column density is $W_\lambda = (21.0 \text{ mÅ})(\mathrm{N_{SiIII}}/10^{12} \text{ cm}^{-2})$. Since the Si III line is so strong, saturation, both resolved and unresolved, is often an issue. For a Gaussian profile, the Si III optical depth at line center is $\tau_0 \approx (0.295) N_{12} b_{10}^{-1}$, scaled to a column density $\mathrm{N_{SiIII}} = (10^{12} \text{ cm}^{-2}) N_{12}$ and to a doppler width $b_{\mathrm{SiIII}} = (10 \text{ km s}^{-1}) b_{10}$, chosen to reflect the turbulence and velocity components that often broaden HVC metal-line absorbers. Typical HVCs exhibit Si III absorption over an extended velocity range,

$\Delta v = 40 - 100$ km s^{-1}, far broader than any single component would allow. Indeed, the curves of growth derived for low metal ions in HVC Complex C (CSG03, CSG07) range from $b \approx 7$–18 km s^{-1}, consistent with non-thermal line widths. Given these large velocity dispersions, we expect Si III line saturation to set in at column densities $N_{SiIII} > (3.4 \times 10^{12}$ cm$^{-2})b_{10}$ in each STIS/E140M resolution element.

In cases where saturation is clearly present in a line profile, we adopt the measured AOD value as a lower limit to N(Si III). The E140M data have a resolution of 7 km s^{-1}, allowing us to search for saturation in the unbinned data. If saturation is present in only one pixel in unbinned E140M data, its effects will not be apparent in the data binned to three pixels. In these cases, we adopt the AOD value as a lower limit. Searching for unresolved saturation in the final G140M profiles is more difficult, because those data are analyzed at their full resolution. To estimate the likelihood of unresolved saturation in HVCs detected in G140M data we begin by examining the normalized flux at the trough of all high-velocity Si III features in the binned E140M datasets. We then determine whether saturation is present in those features in the unbinned data. For normalized fluxes 25% or below at the absorption-line trough in the binned data, saturation is present in the unbinned data in almost all cases. For fluxes above that level, saturation is absent in all but a couple of cases. The G140M data have a similar resolution to the E140M data binned to three pixels, so we adopt 0.25 as the trough normalized flux, below which saturation is likely. In those cases where an HVC has a normalized flux below 0.25 at its trough, we adopt the AOD value as the lower limit to N_{SiIII}. This approach gives reasonable confidence in detecting saturation down to resolutions of 7 km s^{-1}, but reveals little information on saturation over more narrow velocity ranges.

Tables 1 and 2 show the Si III column density measurements of all 90 high velocity components detected in 53 of 58 surveyed sight lines, including target Galactic coordinates, velocity range of the HVC, and equivalent width for the E140M and G140M datasets, respectively. In only a few sight lines did we fail to detect high-velocity Si III. In order to determine a (3σ) upper limit to high-velocity Si III in those sight lines, we first determined whether high-velocity gas was present in any other absorption lines. In two sight lines, 3C 273 and PKS 1302-102, high-velocity O VI has been detected (S03; CSG05) and we adopted the O VI velocity range to establish an upper limit on Si III features. If no HVC of any kind was detected in a sight line, we assumed a typical HVC velocity width of 100 km s^{-1} to establish upper limits. Typically, there is little difference in signal-to-noise (S/N) ratio across 4–5 Å, except for the Mrk 1383 profile where the blueward side is slightly more noisy. Table 3 shows these 5 sight lines where high-velocity Si III is not detected, along with upper limits on N_{SiIII}. Notes on individual sight lines from this survey are presented in Appendices A and B.

4. DISCUSSION

4.1. *Distribution and Covering Factor*

From our sample of 58 sight lines, we can make an estimate of the sky covering factor of high-velocity Si III absorption. We detected high-velocity Si III in 53 of the 58 sight lines, translating to a covering factor of $91 \pm 4\%$. In total, we found 90 HVC velocity components. The error bar corresponds to the possibility that we have misinterpreted Si III absorption in ± 2 sight lines. Interestingly, high-velocity Si III is detected in all 25 of the sight lines with G140M data. In the targets covered by E140M data, we detected high-velocity Si III in 28 of 33 sight lines or $85 \pm 6\%$. Since there are several low-significance detections of weak HVCs, a better estimate of sky covering factor can be obtained by choosing a column density cutoff. If we choose a cutoff of $\log N_{SiIII} = 12.50$ for the combined HVC column density per sight line, the covering factor drops to $84 \pm 4\%$ (49 of 58), with a detection rate of $82 \pm 6\%$ (27 of 33) in the E140M datasets and $88 \pm 8\%$ (22 of 25) in the G140M datasets. These Si III covering factors agree with the value of $81 \pm 5\%$ found in our previous paper (Shull et al. 2009). The HVC sky covering factor has been investigated in other ions as well. The *FUSE* survey (S03) of high-velocity O VI found a covering factor of 59% in the full survey, and 85% if one considers only the highest-S/N datasets. Where higher column density gas was probed, the covering factor was measured at 37% down to column density $N_{HI} \gtrsim 7 \times 10^{17}$ cm^{-2} (Murphy, Lockman, & Savage 1995). This lower covering H I fraction suggests that the HVCs have extended atmospheres of ionized gas, which is best probed by UV resonance lines such as Si III or O VI.

Although the high HVC detection rate of Si III indicates widespread coverage of ionized gas on the sky, there is some evidence that the gas can be clumpy on small scales. Consider the sight-line pair 3C 273 and Q 1230+0115, separated by less than 1°. Towards Q1230+0115, there are two narrow HVC features that can be detected in Si III, as well as in other absorption lines. These features are absent in the 3C 273 spectrum, which is among the highest-S/N spectra in this survey. The narrowness of these absorption features and their absence in a spectrum along a nearby sight line suggests that they are relatively small clumps. Located 5° away from this close pair is the sight line to PG 1216+069, which shows positive high-velocity absorption in multiple absorption lines, but with a completely different velocity profile than the HVCs toward Q1230+0115.

In several other cases, close sight line pairs show similar absorption, indicating that in many cases the high-velocity gas is more extended. The sight lines to Mrk 1044 and NGC 985 are separated by 1.1°. Each sight line shows weak negative high-velocity Si III over $-250 < V_{LSR} < -150$ km s^{-1}, with equivalent widths of 79 ± 17 mÅ and 51 ± 10 mÅ, respectively. The absorption toward NGC 985 having a slightly wider feature over two components. The sight lines to PG 1049-005 and PKS 1103-006 are separated by 3.7°, each showing very strong positive high-velocity features with similar velocity structure in their Si III profiles.

4.2. *The HVC Complexes*

One of the more extended high-velocity features in the sky is the collection of HVCs in the quadrant of the sky comprising Complexes A, C, K, and M, along with the Milky Way's Outer Arm. These Complexes are all roughly connected in velocity, extending out beyond $V_{LSR} \approx -200$ km s^{-1}. It is fortuitous that this part

of the sky is pierced by numerous strong extragalactic sources for absorption-line studies. Figure 3 plots the sight line locations in this survey for the region of sky $180° \geq l \geq 50°$ and $70° \geq b \geq 20°$ together with contours of $N_{\rm HI}$ from the LDS over the velocity range $-210 < V_{\rm LSR} < -90$ km s^{-1}. In the plotted region we have investigated 19 sight lines, nearly one-third of the total from this survey. Even though H I 21-cm emission is detected in only 9 of the 19 sight lines at $N_{\rm HI} \geq 1 \times 10^{19}$ cm^{-2} (roughly the sensitivity of the LDS) over the velocity range $-210 < V_{\rm LSR} < -90$ km s^{-1}, we detected high-velocity Si III in all 19 of these sight lines over some portion of that velocity range. Even the sight lines to PG 1444+407 and Mrk 478, which are separated by $\sim 5°$ and lie $\gtrsim 15°$ from any region of Complex C with $N_{\rm HI} > 10^{19}$ cm^{-2}, show clear Si III absorption at similar velocity. It should be noted, however, that NGC 4051, one of the sight lines without high-velocity Si III absorption, lies just outside the map boundary at $(l, b) = (148.89°, 70.09°)$ within a few degrees of 21-cm emission from Complex M.

The extended Si III absorption probably traces thinner ionized portions of these extended HVC complexes, or a hotter envelope outside the cooler regions of high $N_{\rm HI}$. The second possibility seems to be contrary to the distribution of O VI observed by FSW06. They claim significant non-detections of O VI along sight lines only a few degrees away from the 21-cm emission of these HVC Complexes, suggesting that the hot layer is closely confined to the Complexes. We confirm this trend along 19 sight lines near the HVC Complexes shown in Figure 3. We examined 10 sight lines in this region that contain Si III HVCs at velocities similar to the HVC Complexes, yet outside the $N_{\rm HI} = 1 \times 10^{19}$ cm^{-2} contour. Of five sight lines with viable *FUSE* data covering O VI (PG 1444+407, Mrk 478, H 1821+643, VII Zw118, PG 0953+414), we detect high-velocity O VI at the same velocity in only one case (H 1821+632). In the other four sight lines containing high-velocity Si III but no O VI, the Si III detections are weak. If Si III is entrained in an extended hot envelope to the HVC Complexes, one possible explanation for the lack of O VI may simply be the lower sensitivity to high-velocity gas in the weaker O VI line. (The *FUSE* data generally have lower S/N than STIS.) Alternatively, if the hot O VI-bearing gas is confined to the vicinity of the HVC Complexes, then the Si III gas may trace much lower column density regions in the HVC Complexes.

The fact that 19 of the 58 (33%) sight lines considered in this study lie within a region covering only $\sim 10\%$ of the sky does not significantly bias our results. Although we calculate a $91 \pm 4\%$ covering factor based on the full sample of 58 sight lines, the covering factor only drops to 87% if we ignore the sight lines within the region plotted in Figure 3.

4.3. *Kinematics*

Another topic that can be explored with this survey is the kinematics of the detected Si III HVCs. In Figure 4 we show the locations of the 58 sight lines analyzed in this study, color-coded according to whether the detected HVCs are blueshifted or redshifted. This plot includes five sight lines where no high-velocity Si III is detected. Also labeled are the Local Group barycenter at $(\ell, b) = (147°, -25°)$ (Karachentsev & Makarov 1996) and the direction of the Milky Way's motion, $(\ell, b) = (107°, -18°)$ at $V = 90$ km s^{-1} (Einasto & Lynden-Bell 1982) with respect to the Local Group barycenter.

As seen in our previous studies of HVC kinematics (CSG05) and noted by Shull et al. (2009), the Si III HVC kinematics shows a segregation by velocity in a dipole pattern according to Galactic longitude. With a few exceptions, Si III HVCs at negative velocity are at $0° < l < 180°$ and Si III HVCs at positive velocity are at $180° < l < 360°$. A similar dipole pattern has been observed in high-velocity O VI (S03), highly-ionized HVCs (CSG05, FSW06), and in high-velocity H I. Such a pattern can be explained to first order, by several models that decouple the HVCs from rotation of the Galactic disk. CSG05 showed that a simple model of infall from a non-rotating spherical shell of clouds produces the general segregation trend, but not the absolute LSR velocities. Models with no lag do not work. If the clouds were rotating with the galaxy, they would not be classified HVCs in the first place.

Most previous HVC models assume that the circular velocity remains constant on cylinders, as one moves above the Galactic plane. A velocity lag has recently been noted in the Sloan Digital Sky Survey of ∼200,000 F and G stars (Ivezić et al. 2008), and a circular velocity lag in halo rotation has also been seen in external spiral galaxies (Collins, Benjamin, & Rand 2002). The general pattern can be explained by any of several models in which the HVCs are unconnected, or at least nearly so, to disk rotation. Simple models that produce this dipole pattern include radial infall from non-rotating HVCs, or a slowing rotation rate with height of the Galactic Disk.

4.4. *Ionization Modeling*

Figure 5 shows the Si III column densities of all 90 HVC velocity components analyzed here vs. Galactic longitude and latitude. No clear trends are seen, other than possible peaks in Si III column densities around $\ell = 80 - 120°$ and $\ell = 260 - 300°$. The line saturation in stronger components makes it difficult to make more specific identifications of these features. Studies of weaker lines from other ions should help.

Averaging high-velocity Si III absorption over all sight lines, we found a mean column density $\langle \log N_{\rm SiIII} \rangle = 13.19 \pm 0.45$ (median 13.29). If we treat each velocity component independently, we find $\langle \log N_{\rm SiIII} \rangle = 12.92 \pm 0.46$ (median 12.91). Thus, the typical HVC seen in Si III has a column density $12.5 < \log N_{\rm SiIII} < 13.5$. We scale to a metallicity of 20% solar, adopting a solar abundance (Asplund et al. 2005) of $({\rm Si/H})_\odot = 3.24 \times 10^{-5}$. The median Si III column density corresponds to $N_{\rm HII} \approx (6 \times 10^{18}$ cm$^{-2})(Z_{\rm Si}/0.2Z_\odot)^{-1}$ as the column of ionized low-metallicity gas. These values are similiar to those inferred from the HVCs observed in O VI (Sembach et al. 2003).

In a recent paper, Shull et al. (2009) analyzed a subset of 83 HVC and IVC absorbers with Si II, Si III, and Si IV data toward 37 active galactic nuclei at high latitude. They detected interstellar Si III λ1206.50 absorption in numerous high-velocity clouds (61 HVCs along 30 sight lines) and intermediate-velocity clouds (22 IVCs along 20 sight lines). The fractional HVC sky coverage is large ($81 \pm 5\%$ for 30 out of 37 directions) with Si III optical

depth typically 4–5 times that of O VI λ1031.926. By assuming that Si II, Si III, Si IV, and H I are photoionized, Shull et al. (2009) constrained the mean photoionization parameter in the low halo to be $\langle \log U \rangle = -3.0^{+0.3}_{-0.4}$, approximately ten times lower than in the low-redshift IGM (Danforth & Shull 2008). The metallicities in a subset of these HVCs derived from [Si II/H I] and [O I/H I] are 10–30% solar, whereas values found from all three silicon ions are lower in the pure-photoionization models. These formally lower metallicities, $\langle \log (Z_{\rm Si}/Z_{\odot}) \rangle = -2.1^{+1.1}_{-0.3}$ in 17 HVCs and $-1.0^{+0.6}_{-1.0}$ in 19 IVCs, are highly uncertain, since some of the higher ions may be collisionally ionized. Thus, we see no reason to challenge the more reliable values from O I and Si II.

The larger HVC covering factor seen in Si III absorption (80–90%) compared to H I emission (37%) suggests that HVCs have extended atmospheres of ionized gas, probably of lower density and shredded by HVC motion through a hot halo medium. Thermal interfaces between the H I cores and the hotter substrate (Fox et al. 2006; CSG04; CSG05) may be responsible for the higher ions (O VI, C IV, N V). Thus, comparing probes of the ionized gas (O VI, Si III) with 21-cm maps (H I) could be quite helpful in understanding the cloud geometry. Significant advances in HVC studies could therefore come from improvements in 21-cm sensitivity, reaching below the current limits of $N_{\rm HI} \approx 10^{18}$ cm^{-2}. As the H I column density within an absorber falls below 10^{18} cm^{-2}, the effects of self-shielding are reduced, and it is more straightforward to apply photoionization models to obtain better estimates of the physical properties of the gas. In many plausible photoionization scenarios, the expected column density of neutral hydrogen accompanying Si III absorbers can exceed 10^{17} cm^{-2}.

In Figure 6, we plot the results of two photoionization models consistent with Si II, Si III, and Si IV column densities. These models were constructed using the photoionization equilibrium code *Cloudy* (Ferland 1998). Figure 6a shows an updated version of a model from Collins et al. (2003), who observed HVCs in Complex C with $N_{\rm HI} = 10^{19.0-20.1}$ cm^{-2}. We modeled a constant-density slab of gas illuminated on one side by a hot-star spectrum, as might be expected for gas near the Galactic plane. The level of incident radiation is chosen so that the ionization parameter $\log U \approx -3.9$, and we assumed a metallicity of 20% solar. The curves represent the cumulative calculated Si II and Si III column densities as one goes into the slab from the illuminated side, as measured by the cumulative H I column density. As expected, the cumulative Si III column density asymptotes, as the Si III ionizing photons ($h\nu \geq 16.34$ eV) are attenuated. Once the slab becomes largely neutral in hydrogen, the dominant ionization species Si II rises linearly with cumulative column density. As in previous photoionization models (Collins et al. 2003), we find neutral fractions $N_{\rm HI}/N_{\rm H} \approx 0.4 - 0.7$ over the column-density range $19 < \log N_{\rm HI} < 20$. In this model, $\log N_{\rm SiIII}$ reaches 13.1 when the neutral hydrogen column $N_{\rm HI} \approx 10^{18}$ cm^{-2}. The total hydrogen column is larger, $N_{\rm H} \approx 12\ N_{\rm HI}$.

Figure 6b shows an ionization model consistent with those of Shull et al. (2009). The level of incident radiation has an ionization parameter $\log U \approx -3.1$, and we assumed a metallicity of 10% solar. As in Figure 6a, the curves represent the cumulative column densities as one moves into the slab. In this model, $\log N_{\rm SiIII}$ reaches 13.5 when $\log N_{\rm HI} \approx 18$, and the total hydrogen column is even larger than in Model (6a), with $N_{\rm H} \approx 70 N_{\rm HI}$. As these models indicate, the Si III HVC absorbers with $\log N_{\rm SiIII} > 14$ likely require gas of lower density if the Si III is photoionized. The weakest detectable Si III absorbers with $\log N_{\rm SiIII} \leq 12$, may be associated with higher density gas, or diffuse gas with $N_{\rm HI} < 10^{17}$ cm^{-2}. In fact, regardless of density, the weak Si III absorbers are likely associated with H I column densities below the current detection limits for H I 21-cm emission.

The $\log U = -3.1$ model (Figure 6b) is more consistent with the analysis and ionization models of Shull et al. (2009). In those studies, the Si III HVC absorbers with $\log N_{\rm SiIII} = 12.5$ and 13.5 correspond to neutral column densities $N_{\rm HI} = 5 \times 10^{15}$ cm^{-2} and 6×10^{16} cm^{-2}, respectively. The lower neutral fractions, $N_{\rm HI}/N_{\rm H}$, compared to the Complex-C models of CSG03 arise because the H I column density in those models was much larger and the neutral fraction higher. The assumed gas densities in the CSG03 models were a factor of 4 higher. Although estimates of ionized gas scaled from Si III (Shull et al. 2009) remain reasonably similar for assumed values of metallicity and photoionization conditions, the corresponding H I may vary considerably. In these constant-density *Cloudy* models, the ionizing flux is slowly attenuated with column density, but the neutral fraction remains rather constant at $\log N_{\rm HI} \leq 17.5$. Therefore, just as Si III is proportional to H II, it also remains proportional to H I at low column densities.

5. CONCLUSIONS

For this work, we have assembled all known *HST*-STIS E140M and G140M datasets for extragalactic targets covering the Si IIIλ1206.50 line. This line is one of the strongest for HVC studies, and it lies in a part of the spectrum that is typically uncontaminated by higher-redshift IGM absorption systems. After applying selection criteria, our sample was narrowed to 58 AGN targets. Of those datasets, 33 were STIS/E140M spectra covering 1150–1700 Å and 25 were G140M spectra that covered some portion of the spectrum around the Si III line. We measured velocity extents and Si III column densities for a total of 90 detected HVC absorption features. From those measurements, we arrived at the following conclusions:

1. *Ultraviolet absorption spectra provide the most sensitive probes of ionized HVCs.* We can detect high-velocity Si III in low column density ($N_{\rm HI} \approx 10^{17}$ cm^{-2}) portions of the HVC Complexes, well below current senstivity levels in 21-cm emission.

2. *The sky covering fraction of high-velocity Si III λ1206.5 absorption is 80–90%.* This covering fraction is considerably higher than that (37%) seen in 21-cm emission. Because of its intrinsic strength, high-velocity Si III is detected in 53 of 58 sight lines, with 59% of the HVCs showing negative LSR velocities. If one sets the Si III column density cutoff at $\log N_{\rm SiIII} = 12.50$, comparable to the detection limit of the poorer data, the covering factor drops to 84 ± 4% (49 of 58 sight lines). The gas

appears to be clumpy in some cases, as evidenced by the sight-line pair 3C 273/Q 1230+0115 (separated by $\lesssim 1^\circ$) that show very different absorption profiles. In other close pairs, the absorption characteristics are similar, indicating extended cloud structure.

3. *High-velocity gas appears near the HVC Complexes.* A significant number (19 of 58) of the sight lines probe the region occupied by Complexes A, C, K, M, and Milky Way Outer Arm. Even though high-velocity H I 21-cm emission is detected in only 9 of the 19 sight lines with $N_{HI} \geq 1 \times 10^{19}$ cm^{-2}, we detect Si III HVCs in all 19 sight lines, in some cases quite far ($\sim 15^\circ$) from any H I emission. The distribution of Si III near the HVC Complexes is somewhat different than that of O VI, which is typically not detected more than a few degrees from the HVC Complexes.

4. *The Si III HVC absorber kinematics exhibit a redshift/blueshift dipole.* As first seen in our previous studies of HVC kinematics (CSG05), we detect a dipole in the pattern of the Si III HVCs split across the direction of the Galactic anti-center. This pattern is seen through a segregation of redshifted and blueshifted absorbers across the Galactic rotation axis at $\ell = 180^\circ$ and is consistent with a lag in rotation velocity above the Galactic plane. Such a pattern can be explained by several models that decouple the HVCs from rotation of the Galactic disk.

What do these results indicate for the ionization state and total hydrogen column densities of the HVC population? With STIS/E140M, the Si III λ1206.50 absorption line is sensitive to column densities at or below $N_{SiIII} \approx (10^{12}$ cm$^{-2})N_{12}$, corresponding to equivalent width $W_\lambda = (21.0$ mÅ$)N_{12}$. Our best STIS data reach equivalent widths of 10 mÅ, or $\log N_{SiIII} = 11.7$. These limits may improve with new data from the Cosmic Origins Spectrograph (COS) recently installed on *HST*. The COS instrument is capable of obtaining far-UV spectra at S/N ≥ 40 and 15 km s^{-1} resolution, and it should be sensitive to Si III equivalent widths as low as 6 mÅ or column densities $\log N_{SiIII} \approx 11.7$.

As noted above, the Si III ultraviolet absorption line is a sensitive probe of ionized gas, sensitive to total hydrogen column densities $N_H \approx 10^{17}$ cm^{-2}, for gas at 20% solar metallicity. Analysis of metal ions such as O VI, C IV, Si III in these HVCs currently provides our most sensitive probe of low-metallicity gas from the Galactic halo – perhaps the "cold-mode" accretion that replenishes material used up by star formation in the disk (Keres et al. 2005; Dekel & Birnboim 2006). Extending the 21-cm studies down to $\log N_{HI} \approx 17$ would better match these UV-line sensitivities and help to sharpen our estimates of ionization conditions and mass-inflow rates. These sensitivities should be possible with new radio facilities and receivers, including the ALFA survey with Arecibo (Giovanelli et al. 2005), the Greenbank Telescope, and various precursors of the Square Kilometer Array.

Our group's research support at the University of Colorado for UV studies of the IGM and Galactic halo gas comes from COS grant NNX08-AC14G and STScI spectroscopic archive grants (AR-10645.02-A and AR-11773.01-A). We also acknowledge theoretical support from NSF grant AST07-07474.

REFERENCES

Asplund, M., Grevesse, N., & Sauval, A. J. 2005, in Cosmic Abundances as Records of Stellar Evolution and Nucleosynthesis, ASP Conf. Ser. 336, 25
Bowen, D. V., Pettini, M., & Blades, J. C. 2002, ApJ, 580, 169
Blitz, L., Spergel, D. N., Teuben, P. J., Hartmann, D., & Burton, W. B. 1999, ApJ, 514, 818
Cen, R., & Ostriker, J. P. 1999, ApJ, 514, 1
Collins, J. A., Benjamin, R. A., & Rand, R. J. 2002, ApJ, 578, 98
Collins, J. A., Shull, J. M., & Giroux, M. L. 2003, ApJ, 585, 336 (CSG03)
Collins, J. A., Shull, J. M., & Giroux, M. L. 2004, ApJ, 605, 216 (CSG04)
Collins, J. A., Shull, J. M., & Giroux, M. L. 2005, ApJ, 623, 196 (CSG05)
Collins, J. A., Shull, J. M., & Giroux, M. L. 2007, ApJ, 657, 271 (CSG07)
Danforth, C. W., & Shull, J. M. 2008, ApJ, 679, 194
Dekel, A., & Birnboim, Y. 2006, MNRAS, 383, 2
Einasto, J., & Lynden-Bell, D. 1982, MNRAS, 199, 67
Fox, A. J., Savage, B. D., Wakker, B. P., Richter, P., Sembach, K. R., & Tripp, T. M. 2004, ApJ, 602, 737
Fox, A. J., Savage, B. D., Wakker, B. P., Tripp, T. M., & Sembach, K. R. 2005 ApJ, 630, 332
Fox, A. J., Savage, B. D., & Wakker, B. P. 2006, ApJS, 165, 229 (FSW06)
Gabel, J. R., et al. 2003, ApJ, 583, 178
Ganguly, R., Sembach, K. R., Tripp, T. M., & Savage, B. D. 2005, ApJ, 157, 251
Gibson, B. K., Giroux, M. L., Penton, S. V., Stocke, J. T., Shull, J. M., & Tumlinson, J. 2001, AJ, 122, 3280
Giovanelli, R., et al. 2005, AJ, 130, 2498
Hartmann, D., & Burton, W. B. 1997, Atlas of Galactic Neutral Hydrogen (Cambridge: Cambridge Univ. Press)
Ivezić, Z., et al. 2008, ApJ, 684, 287
Karachentsev, I. D., & Makarov, D. A. 1996, AJ, 111, 794
Keeney, B. A., Danforth, C. W., Stocke, J. T., Penton, S. V., Shull, J. M., & Sembach, K. R. 2006, ApJ, 646, 951
Keres, D., Katz, N., Weinberg, D. H., & Davé, R. 2005, MNRAS, 363, 2
Morton, D. C., 2003, ApJS, 149, 205
Murphy, E. M., Lockman, F. J., & Savage, B. D. 1995, ApJ, 447, 642
Murphy, E. M., et al. 2000, ApJ, 538, L35
Nicastro, F., et al. 2002, ApJ, 573, 157
Nicastro, F., et al. 2003, Nature, 421, 719
Pagel, B. E. J. 1994, in The Formation and Evolution of Galaxies, ed. C. Munez-Tunón & F. Sánchez (Cambridge: Cambridge Univ. Press), 149
Penton, S. V., Stocke, J. T., & Shull, J. M. 2004, ApJS, 152, 29
Putman, M. E., et al. 2009, How do galaxies accrete gas and form stars? Astro2010 Science White Paper, http://adsabs.harvard.edu/abs/2009astro2010S.241P
Richter, P., et al. 2001, ApJ, 559, 318
Savage, B. D., & Sembach, K. R. 1991, ApJ, 379, 245
Sembach, K. R., Savage, B. D., Lu, L., & Murphy, E. M. 1999, ApJ, 515, 108
Sembach, K. R., et al. 2003, ApJS, 146, 165
Sembach, K. R., Tripp, T. M., Savage, B. D., & Richter, P. 2004, ApJS, 146, 165
Shull, J. M., Tumlinson, J., & Giroux, M. L. 2003, ApJ, 594, L107
Shull, J. M., Jones, J. R., Danforth, C. W., & Collins, J. A. 2009, ApJ, 700, 754
Thom, C., Peek, J. E. G., Putman, M. E., Heiles, C., Peek, K. M. G., & Wilhelm, R. 2008, ApJ, 684, 364
Tripp, T. M., et al. 2003, AJ, 125, 3122
Tumlinson, J., Shull, J. M., & Giroux, M. L. 2005, ApJ, 620, 95
Vázquez, G. A., et al. 2004, ApJ, 600, 162
Wakker, B. P., et al. 1999, Nature, 402, 388
Wakker, B. P., et al. 2003, ApJS, 146, 1
Wakker, B. P., et al. 2007, ApJ, 670, L113
Wakker, B. P., et al. 2008, ApJ, 672, 298
Wakker, B. P., & van Woerden, H. 1991, A&A, 250, 509
Wakker, B. P., & van Woerden, H. 1997, ARA&A, 35, 217
Zech, W. F., Lehner, N., Howk, J. C., Dixon, W. V. D., & Brown, T. M. 2008, ApJ, 679, 460

APPENDIX

E140M SIGHT LINES

3C 273.— High-velocity gas toward 3C 273 has been well studied using both *HST*-STIS and *FUSE* data (S03, CSG05). There is a weak high-velocity O VI absorber in this sight line, but no corresponding feature is detectable in any other absorption line, including Si III. To establish an upper limit on the high-velocity Si III column density, we use the velocity extent of the high-velocity O VI feature, $V_{\rm LSR} = 105$ to 240 km s^{-1}.

3C 351.— 3C 351 is a Complex C sight line and was investigated by Tripp et al. (2003) and CSG07. The sight line also pierces Complex K and the High-Velocity Ridge at slightly lower and higher velocities than Complex C, respectively. These three high-velocity features are resolvable in many absorption lines. In Si III, however, the Complex C and K features are saturated and blended with lower-velocity absorption. We therefore measure these components as one single Complex C/K component and determine a lower limit to $N_{\rm SiIII}$.

H 1821+643.— The H 1821+643 sight line passes through the Milky Way Outer Arm and near Complexes C and K (Tripp et al. 2003). S03 detect high-velocity O VI all the way out to $V_{\rm LSR} = -285$ km s^{-1}. Lines of lower ionization stage, however, do not extend to nearly as large a negative velocity. In contrast to weaker lines where features of Complex C and C/K are well separated, the Si III is heavily saturated and blended in this velocity range. For this reason, we integrate over the full Complex C and K features for the analysis of the Si III line.

HE 0226-4410.— This sight line passes through a highly ionized HVC that has been investigated in detail (CSG05, Fox et al. 2005). The HVC is detected in multiple absorption lines.

HS 0624+6907.— This sight line passes through a detectable H I column of the Outer Arm. The Outer Arm feature is clearly detectable in Si III over $V_{\rm LSR} = -127$ to -90 km s^{-1}. Although this feature is not detected in O VI (S03), it is detectable in multiple ionization stages in the E140M bandpass ranging from O I to C IV. A weak Si III feature (4σ) is also present over $V_{\rm LSR} = 100$ to 135 km s^{-1}. This weak feature is not detected in any other absorption line. Although we cannot identify it as an IGM feature, the possibility cannot be ruled out.

HS 1700+6416.— The HS 1700+6416 sight line passes through a broad weak column of Complex C. Based on the H I (LDS) data toward this sight line, we cannot measure the H I column density of Complex C to better than 3σ, although a feature does seem to be present. The Complex C feature is detected in multiple absorption lines, most of which are saturated, including the Si III line.

Mrk 279.— Mrk 279 is an important Complex C sight line, discussed in detail by CSG03 and CSG07. There are two Complex C components detected in H I emission, the lower velocity of which blends with intermediate and low velocity gas. We take the approach of CSG07 and analyze only the higher-velocity Complex C component. This component is detected in multiple absorption lines, with the Si III absorption extending to slightly more negative velocity than the low ions. We integrate the full Si III feature for the column density measurement.

Mrk 335.— The Mrk 335 sight line shows a complicated Si III profile with four possible distinct high-velocity features. All these features are detected in other absorption lines, except the highest velocity feature, which may have corresponding detections in other lines at slightly offset velocity. The broadest feature centered at $V_{\rm LSR} \approx -325$ km s^{-1} is also detected in O VI (S03). The saturated feature centered at $V_{\rm LSR} \approx -100$ km s^{-1} overlaps in velocity with a detected high-velocity O VI feature. However, the O VI feature extends to more negative velocity than the Si III feature by nearly 100 km s^{-1}, suggesting that they may not be completely associated with one another.

Mrk 509.— This sight line is one of the earliest to be examined, defining the category of highly ionized HVCs (Sembach et al. 1999). CSG04 studied high velocity gas in this sight line recently and measured ion column densities for two negative-velocity highly ionized HVC components, detectable in ions ranging from C II through O VI. The Si III measurements are updated here, and we also detect a positive high-velocity wing to the Si III profile. Although it does not extend to as high velocity, this feature may be related to the O VI wing presented by S03 that extends out to $V_{\rm LSR} = 200$ km s^{-1}.

Mrk 876.— Mrk 876 is another Complex C sight line investigated by Murphy et al. (2000), CSG03, and CSG07. There are two Complex C components pierced by the sight line to Mrk 876, and they appear saturated and blended together in the Si III profile. The division between the two components is taken at $V_{\rm LSR} = -155$ km s^{-1}, which is the division seen in weaker low ionization lines (e.g. O I and Si II).

Mrk 1383.— Although a weak high-velocity positive O VI wing was detected by S03, we see no evidence of any high-velocity Si III absorption in this sight line. Keeney et al. (2006) detected high-velocity absorption in O VI, C III, C IV and Si IV. We estimate an upper limit on high-velocity N(Si III) by assuming a width of 100 km s^{-1} for any possible feature.

NGC 1705.— This sight line intercepts HVC WW487, which is seen centered at $V_{\rm LSR} \approx 285$ km s^{-1} in both H I data (Wakker & van Woerden 1991) and in multiple absorption lines in the STIS bandpass (Vazquez et al. 2004). The Si III profile shows the WW487 feature and a positive velocity HVC that extends over $V_{\rm LSR} = 100$ to 148 km s^{-1}. The lower-velocity HVC is seen in lines of Si II and C II as well. High-velocity O VI associated with both features was detected by S03. The prominent feature at $V_{\rm LSR} > 400$ km s^{-1} is Si III absorption intrinsic to NGC 1705.

NGC 3516.— The NGC 3516 sight line passes near Complex C, but not through a detectable (21-cm) column of H I. A Si III feature is detected centered at $V_{\rm LSR} \approx -150$ km s^{-1}, a velocity similar to that of Complex C in that vicinity. The feature is also clearly detected in C II λ1334.53, and possibly in weak features of O I λ1302.17 and Si III λ1193.29. This sight line likely probes a low column density portion of Complex C.

NGC 3783.— The Si III profile shows clear negative velocity high-velocity gas spread over two components, the higher-velocity component of which is detectable in H I emission as HVC WW187 (Wakker et al. 2003). The high-velocity gas was first noticed in the STIS data by Gabel et al. (2003). The features are clearly seen as two components in nearly all low ion absorption lines in the E140M bandpass, but are not seen in C IV or Si IV lines.

NGC 4051.— No high-velocity gas is detected in the Si III profile, nor in any other absorption lines. We estimate an upper limit on high-velocity $N_{\rm SiIII}$ by assuming a width of 100 km s^{-1} for any possible feature.

NGC 4593.— High-velocity Si III is detected in this sight line in two unusual narrow features, one centered at $V_{\rm LSR} \approx 100$ km s^{-1} and the other at $V_{\rm LSR} \approx 275$ km s^{-1}. These detections are confirmed by corresponding detections of each feature in Si II λ1260.42, and of the lower velocity feature in C II λ1334.53. The lower-velocity feature appears to extend out to larger positive velocity in the Si III profile. Because this part of the feature is not present in the Si II and C II profiles, we use the velocity extent of the lower ions for the Si III integration.

NGC 5548.— This sight line shows some evidence for high-velocity gas, but the absorption only extends out to $V_{\rm LSR} = -125$ km s^{-1} in the Si III profile. The feature is not seen in low ions, although low ion absorption features do extend out to nearly $V_{\rm LSR} = -100$ km s^{-1}. Although we see absorption out to $V_{\rm LSR} = -125$ km s^{-1} in O VI, it was reported as a high-velocity non-detection by S03. Owing to the weakness of the absorption and the small extent into the "high-velocity" range, we report this sight line as a Si III non-detection. We estimate an upper limit on high-velocity $N_{\rm SiIII}$ by assuming 100 km s^{-1} width for any possible feature.

NGC 7469.— Several high-velocity Si III components are detected in this sight line at negative velocity. Absorption in O VI associated with each of these components is reported by S03. The strong highest-velocity component is detected in a variety of absorption lines ranging in ionization from O I to C IV. We break this strong absorption feature into two components separated at $V_{\rm LSR} = -270$ km s^{-1}. The lowest-velocity component is not detected in low ions, only in the higher ions C IV, Si IV, and Si III.

PG 0953+414.— This sight line passes through a positive velocity HVC that was investigated in CSG05 and Fox et al. (2005). Both Si III and C II λ1334.53 profiles show evidence that this feature consists of two components. We analyze them in that manner for this work. We also detect clear high-velocity absorption at $V_{\rm LSR} \approx -150$ km s^{-1}, where a strong narrow feature is detected in C II and Si II as well, but not in high ions C IV and O VI. As mentioned by CSG05, this feature correlates spatially and kinematically with HVC Complex M, although it does not pass through a detectable H I column of that object. Closer to Galactic absorption, we detect a negative-velocity wing to the Si III profile extending out to $V_{\rm LSR} = -130$ km s^{-1}. This wing is present in low ions, C II and Si II, as well as C IV. This feature may be associated with Galactic absorption, but since it is technically at high velocity, we report it as such.

PG 1116+215.— The positive high-velocity gas in this sight line was first presented in STIS data by Sembach et al. (2004) and thoroughly studied by Ganguly et al. (2005) and CSG05. Although the higher velocity component (130–220 km s^{-1}) is detected in multiple absorption lines ranging in ionization from O I to C IV and O VI, the lower velocity component (90–125 km s^{-1}) is present to a high level of certainty only in Si III and C IV.

PG 1211+143— No high-velocity O VI absorption was detected in this sight line by the S03 survey. However, in Si III, we detect two weak positive high-velocity features. The lower-velocity component is clearly detected in absorption lines of Si II and C II. The weak component at higher velocity is not detected in any other absorption line. We are unable to identify it as an IGM line from this data, nor can it be matched with reported Lyα features in this sight line reported by Tumlinson et al. (2005) and Penton et al. (2004; based on STIS G140M data). We identify the feature as high-velocity Si III.

PG 1216+069.— This sight line shows strong positive high-velocity Si III absorption spread out over at least two components. This feature is detected in C IV over the same velocity extent, and in Si II λ1260.42 over a slightly narrower velocity range. Although not included by S03, owing to IGM Lyβ contamination, the feature seems present in O VI as well. Based on comparisons of absorption profiles, we analyze the feature as two components separated at $V_{\rm LSR} = 234$ km s^{-1}.

PG 1259+593.— This well-studied sight line passes through HVC Complex C (Richter et al. 2001; CSG03; CSG07). We use the saturated Si III profile to place a lower limit on $N_{\rm SiIII}$ for Complex C in this direction. A positive-velocity HVC is detected in O VI by S03 over $V_{\rm LSR} = 100 - 185$ km s^{-1}, but no corresponding Si III absorption is detected here.

PG 1444+407.— Possible high-velocity Si III absorption is seen just blueward of Galactic absorption in this sight line. Although the feature is weak, corresponding high-velocity features are seen in both C II λ1334.53 and C IV λ1548.20 over a similar velocity extent. No corresponding high-velocity O VI was detected in the S03 survey.

PHL 1811.— The complicated high-velocity absorption features in this sight line were presented in CSG05, but a full quantitative analysis was deferred until further data was available. The data presented here include the full STIS exposure. We detect strong high-velocity Si III absorption in four components spread over a wide velocity range at negative $V_{\rm LSR}$. These components are detected in multiple absorption lines ranging in ionization from O I to O VI.

PKS 0312-770.— This sight line passes through the Magellanic Bridge, and strong corresponding high-velocity absorption is seen in multiple absoprtion lines, including Si III λ1206.50. Although not apparent from the Si III line, this feature breaks into two components separated at $V_{\rm LSR} = 285$ km s^{-1} in weaker lines (Shull et al. 2009). We use the velocity structure seen in the weaker lines to establish the velocity range for measurement of the two components in Si III. Good *FUSE* data exists for this sight line, but due to a break in the spectrum, the O VI lines are unavailable.

PKS 0405-123.— A weak ($\sim 4\sigma$) absorption feature just redward of Galactic Si III absorption is detected in this sight line. We do not detect absorption at the same velocity in any other absorption lines in the STIS bandpass. A weak O VI detection at this velocity was presented by S03. The *FUSE* exposure time for this target has been doubled since the work of S03, and we confirm the presence of the high-velocity O VI feature in those data. Based on the corresponding O VI detection and the absence of any known IGM contaminant lines, we adopt the feature in question as a high-velocity Si III detection. Recent COS observations confirm this HVC, with an equivalent width 29 ± 7 mÅ.

PKS 1302-102.— This sight line contains a strong high-velocity O VI feature (S03, CSG05) with no associated absorption in any other ions, including Si III. We use the $V_{\rm LSR} = 200$ to 340 km s^{-1} extent of the O VI feature to establish an upper limit on the Si III absorption.

PKS 2155-304.— This sight line contains a pair of highly ionized HVCs that were among the first to be studied using *HST*-GHRS data (Sembach et al. 1999). *HST*-STIS data for this sight line (Shull, Tumlinson, & Giroux 2003) was analyzed by CSG04, showing absorption in multiple ion stages ranging from C II to O VI. The absorption is detectable as two distict negative-velocity components.

Q 1230+0115.— Two narrow high-velocity Si III features are detected in this sight line centered at $V_{\rm LSR} \approx 125$ and 300 kms^{-1}. These detections are confirmed by associated absorption in multiple lines of Si II, C II, and O I. These features, however, are not detected in the higher ions C IV or Si IV. Wakker et al. (2003) presented *FUSE* O VI data for this sight line, in which associated absorption appears present in the 1031.93 Å line, but not in the 1037.62 Å line.

TON 28.— High velocity Si III absoprtion appears over the velocity range $V_{\rm LSR} = 97$ to 183 km s^{-1}. However, associated absoprtion over that range is not detected in any other lines in the *HST*-STIS bandpass. S03 report a detection in O VI over a nearly identical velocity range, but at low significance ($\sim 3\sigma$). Since we are unable to find any coincident IGM lines at redshifts that could contaminate the Si III line, we adopt this as a high-velocity Si III detection.

TON S210.— These data were taken for a program whose goal was to investigate a compact HVC (CHVC) in this sight line. Definite high-velocity Si III absorption over two slightly blended components is seen, and O VI absorption over the same velocity extent was presented by S03. Absorption out to $V_{\rm LSR} \approx -150$ km s^{-1} is most likely due to an IVC that peaks near $V_{\rm LSR} \approx -80$ km s^{-1}. The lower velocity component centered near $V_{\rm LSR} \approx -180$ km s^{-1} is detectable in lines ranging in ionization from O I to O VI. The higher velocity component centered near $V_{\rm LSR} \approx -240$ km s^{-1} is seen prominently in the higher ions C IV and Si IV, but only weakly, if at all, in singly ionized and neutral species.

UGC 12163.— We detect strong high-velocity absorption in this sight line throughout the negative velocity range out to nearly $V_{\rm LSR} \approx -500$ km s^{-1}. This absorption is seen in ionization stages ranging from O I to O VI. These detections were first reported by CSG05, but the S/N was judged to be too poor to properly disentangle the complicated absorption features. There are at least three high-velocity Si III components present in this sight line that correspond to features seen in other absorption lines. Owing to the complicated absorption profiles, we rely only on the Si III profile to establish integration ranges.

G140M SIGHT LINES

ES 438-G009.— The Si III profile shows complicated, yet strong, positive high-velocity absorption spread over at least two components. Because the spectrum covers only the range 1194–1249 Å, we are unable to confirm the detection with other ion species, nor can we use other lines to better constrain the velocity ranges. We cannot attribute the high-velocity Si III absorption to any redshifted contaminant lines, so we treat this as a high-velocity Si III detection. According to our analysis of unresolved saturation in binned E140M data (see Section 3), the lower velocity component is likely saturated, and we treat the measured $N_{\rm SiIII}$ as a lower limit.

HE 0340-2703.— A narrow feature at positive velocity is detected in the Si III profile for this sight line. Although the limited coverage of the spectrum (1194–1249 Å only) prevents the confirmation of this as a Si III feature from other absorption lines, we cannot attribute this to a redshifted contaminant line based on the redshifted Lyα features that we can detect in the spectrum. We therefore treat this as a high-velocity Si III detection.

HE 1029-1401.— This sight line has excellent data covering the wavelength range 1194–1298 Å. A strong positive high-velocity wing is apparent in the Si III profile and is confirmed by a nearly identical wing seen in the profile of Si II λ1260.42. In the weaker absorption lines of N I λ1200.71 and S II λ1253.80, the lower velocity part of the feature is clearly seen as a single component. Since there is a small hump also seen on the shoulder of the Si III feature, indicating more than one component, we break the high-velocity absorption into two components separated at $V_{\rm LSR} = 178$ km s^{-1}.

HS 1543+5921.— This is a Complex C sight line thoroughly analyzed in CSG07. The data are of good quality and cover a large wavelength range, 1194–1348 Å. In low ions, Complex C can be detected in lines of N I, O I, Si II, S II, and C II. Corresponding Complex C absorption has a quite different appeareance in Si III, lacking any sort of peak near the line centroid. A significant absorption feature at $V_{\rm LSR} \approx -400$ km s^{-1} corresponding to intervening Si II λ1193.29 at $z = 0.0096$ just blueward of the Complex C Si III feature makes continuum fitting near the Si III line difficult. Thus, the Complex C Si III profile may be slightly distorted or contaminated.

IRAS 08339+6517— A strong negative high-velocity feature is present in the Si III profile. The wavelength coverage of the spectrum is limited to 1194–1249 Å, so the high-velocity Si III feature cannot be confirmed with other absorption lines. However the LDS H I 21-cm spectrum shows a portion of this HVC over $-200 < V_{\rm LSR} < -100$ km s^{-1}, at a column density $N_{\rm HI} \approx 2 \times 10^{19}$ cm^{-2}. Although the Si III absorption extends to larger negative velocity, the H I profile confirms this high-velocity detection.

MCG 10.16.111— This sight line has excellent quality data, but over a limited velocity range (1194–1249 Å). In Si III, we see negative high-velocity absorption extending out to nearly $V_{\rm LSR} = -250$ km s^{-1}, which we cannot confirm with other absorption lines. There are numerous Lyα features in this sight line associated with intervening galaxies (Bowen, Pettini, & Blades 2002), but given their strengths in Lyα it is highly unlikely that the Si III profile is contaminated by associated absorption in redshifted metal lines. The H I LDS profile shows an IVC extending out to $V_{\rm LSR} = -70$ km s^{-1}, which may be responsible for some of the high-velocity absorption if the feature is strong enough for saturated wings to blend with the HVC absorption. However, owing to the extension to large negative velocity, we accept this feature as a high-velocity Si III detection.

MRC 2251-178— Data for this sight line are of excellent quality and cover the wavelength range 1194–1298 Å. The sight line intercepts a negative-velocity highly-ionized HVC analyzed in detail by CSG05. In the *FUSE* bandpass, O VI and C II λ1036.34 are detected over the same velocity extent as the negative-velocity Si III HVC. In addition, we detect a positive-velocity wing to the Si III profile that extends out beyond $V_{\rm LSR} = 150$ km s^{-1} that is not detected at a statistically significant level in any other absorption line. The feature seems present at a very low level in the Si II λ1260.42 line, lending some confidence that the Si III feature is real.

Mrk 110— A strong negative high-velocity feature is present in the Si III profile. We are unable to confirm the detection with other absorption lines owing to the limited 1194–1249 Å coverage of the spectrum. Since we cannot identify the feature as a higher-redshift contaminant, we adopt the feature as a high-velocity Si III detection. Our analysis of saturation in binned E140M datasets indicates that saturation in this strong feature is likely, and we therefore adopt the measured $N_{\rm SiIII}$ as a lower limit.

Mrk 478— A weak negative high-velocity wing is present in the Si III profile for this sight line out to $V_{\rm LSR} = -158$ km s^{-1}. The 1194–1298 Å coverage of this spectrum allows the analysis of this feature in additional lines. In Si II λ1260.42, this wing can be detected out to $V_{\rm LSR} = -135$ km s^{-1} at a low but statistically significant level. S03 report an O VI HVC in this sight line over $340 < V_{\rm LSR} < 435$ km s^{-1}. We do not detect a corresponding feature in the Si III line.

Mrk 926— Clear negative high-velocity absorption is present in the Si III profile for this sight line. This detection was reported in the highly ionized HVC study of CSG05, but was dropped from thorough analysis owing to the poor quality of its *FUSE* data. Although the STIS spectrum covers the range 1194–1298 Å we cannot confirm the Si III detection since the negative high-velocity range of the strong Si II λ1260.42 line is contaminated by Galactic S II λ1259.52. However, the poor-quality *FUSE* data do provide some evidence of associated absorption features in both O VI and C II λ1036.34. In addition, there are no known higher-redshift contaminants that could be responsible for the feature in the Si III profile. We therefore adopt this as a high-velocity Si III detection.

Mrk 1044— Good quality data exist for this sight line from 1194–1298 Å and 1540–1594 Å, which allows the analysis of the C IV doublet. An obvious negative high-velocity feature is present in the Si III profile. This feature, however, is not present in the C IV λ1548.20 line. In addition, we cannot confirm the detection with the Si II λ1260.42 line due to contamination from Galactic S II λ1259.52. However, a very similar absorption feature is seen towards NGC 985, which is only 1.1° away from this sight line. Since there are no known higher-redshift contaminants that could affect the Si III profile, we adopt it as a high-velocity Si III detection.

Mrk 1513— This sight line contains highly ionized negative high-velocity gas studied thoroughly by CSG05. The feature is clearly present in the Si III line, as well as the O VI and C III λ977.02 lines in *FUSE* data of fair quality. It is not present at a statistically significant level in C II λ1036.34. The STIS data quality is superior to the *FUSE* data, and although the spectrum covers 1194–1298 Å, we cannot confirm the feature in Si II λ1260.42 due to contamination from Galactic S II λ1259.52. The Si III profile indicates multi-component absorption, and we thus break the feature into three separate components.

NGC 985— High-velocity Si III is present in this sight line spread over two negative velocity components. The spectrum covers 1194–1298 Å, allowing analysis of the Si II λ1260.42 line. Most of the corresponding velocity range of the prospective HVC is blocked by Galactic S II λ1259.52, but the lower velocity component is clearly present. In addition, a similar absorption feature is seen towards Mrk 1044, which is 1.1° from this sight line. Since there are also no known higher redshift contaminants that could affect the Si III profile, the two components are thus accepted as high-velocity Si III detections.

PG 0804+761— High quality STIS data for this sight line are available (Richter et al. 2001) over the wavelength range 1194-1298 Å. The H I LDS profile for this sight line shows three components: a Galactic feature, an IVC over $-80 < V_{\rm LSR} < -40$ km s^{-1}, and broad low-level high velocity absorption beginning at $V_{\rm LSR} = -80$ km s^{-1} and extending out to $V_{\rm LSR} \approx -170$ km s^{-1}. These three features are well blended in the Si III profile, and we use the $V_{\rm LSR} = -80$ km s^{-1} point to mark the cutoff for integration of the high-velocity feature. The high-velocity feature is also present in the profile of Si II λ1260.42 out to $V_{\rm LSR} = -150$ km s^{-1}, where the feature becomes blended with S II λ1259.52. This feature was not detected in the survey of high-velocity O VI (S03).

PG 1049-005— The Si III profile shows strong positive high-velocity absorption, spread over two components. Although the wavelength coverage is limited (1194–1249 Å), the lower velocity HVC component is so strong that it can be detected in the weak N I λ1200.71 line, confirming the high-velocity Si III detection. The higher velocity HVC component can only be detected in Si III, so its detection as high-velocity Si III cannot be confirmed. We note that the relatively high redshift of this QSO target ($z = 0.3599$, one of the highest in this survey) allows for the larger likelihood of contamination by IGM absorbers. The limited coverage of the spectrum prevents a thorough investigation of this possibility.

PG 1351+640— This sight line pierces HVC Complex C and has been discussed in both CSG03 and CSG07. In the *FUSE* bandpass, this high-velocity feature can be detected in lines of Fe II, Si II, and O VI. Complex C is highly saturated in the Si III line and we take its measurement as a lower limit on N(Si III).

PKS 1004+130— The Si III profile of this sight line shows a strong positive high-velocity feature. Owing to the limited 1194–1249 Å coverage of the spectrum, we cannot confirm its detection with other absorption lines. Based on supplementary *FUSE* and GHRS/G140L data, we cannot identify the feature in the Si III profile as a contaminant. We therefore adopt it as a high-velocity Si III detection. This sight line was reported as an O VI non-detection by S03. However, the O VI λ1031.926 profile shows an absorption feature with an identical velocity extent and trough as the Si III feature, although with a slightly different overall appearance. This feature is not present in O VI λ1037.62, although that part of the spectrum is strongly contaminated by H_2 lines, leading to the S03 classification as an O VI non-detection. Wakker et al. (2003) suggest that the feature in the O VI profile may be O III λ832.93 at $z = 0.2398$. The detection of corresponding high-velocity Si III opens up the possibility that the feature in the *FUSE* spectrum may actually be high-velocity O VI.

PKS 1103-006— The data quality for this sight line is sub-par, but sufficient to detect the strong positive high-velocity absorption in the Si III profile. Owing to the limited 1194–1249 Å wavelength coverage, we are unable to confirm this detection with other absorption lines. The relatively high redshift of this target ($z = 0.423$) increases the likelihood of contamination by IGM lines, but from the available data we cannot identify a definite contaminant. Thus, we accept the feature as a detection of high-velocity Si III.

PKS 2005-489— A strong positive high-velocity wing to Galactic absorption is seen in the Si III profile for this sight line. The data quality is excellent, with coverage extending from 1194–1298 Å. In addition to this HVC being detected in O VI (S03), it can also be detected as a wing in Si II λ1260.42 and N I λ1200.71. Keeney et al. (2006) also reported high-velocity O VI and C III (the C IV and Si IV spectra were not available in STIS/E140M spectra,] owing to the 2004 failure.)

Q 1831+731— The data quality for this sight line is good, but the wavelength coverage is limited to the 1194–1249 Å range. A fairly strong negative high-velocity wing to Galactic absorption is seen in the Si III profile extending out to $V_{\rm LSR} \approx -200$ km s^{-1}. Given the limited wavelength coverage, we cannot conclusively confirm this feature with other absorption lines. The N I λ1199.55 line shows a negative velocity wing extending out to possibly $V_{\rm LSR} \approx -150$ km s^{-1}, although not at a level of sufficient significance. Since we cannot identify a higher-redshift contaminant that could be affecting the Si III profile, we accept this as a high velocity Si III detection.

RXSJ 01005-511— Strong positive high-velocity absorption is seen over possibly two components in the Si III profile. The wavelength coverage of the spectrum, 1194–1298 Å allows access to additional absorption lines such as Si II λ1260.422. In this Si II line, the two-component structure is more pronounced, with the feature broken up into a positive-velocity wing and a distinct component that peaks at $V_{\rm LSR} \approx 175$ km s^{-1}. The feature is not present in N I λ1200.71. We use the component structure in the Si II profile for the velocity ranges used to measure Si III.

TON 730— A weak negative high-velocity wing extending out to $V_{LSR} = -140$ km s^{-1} can be detected in the Si III profile at the 3σ level in this sight line. Owing to the limited wavelength coverage, we cannot confirm the detection with other absorption lines. Since there are no known higher-redshift contaminants that could be responsible for the absorption, we adopt it as a high-velocity Si III detection. However, the fact that it does not extend to velocities far beyond Galactic absorption makes this a somewhat questionable detection. Given the uncertainties in calibrating the LSR velocity scales of these particular spectra, it is possible that the wing lies at a lower velocity and is not high-velocity gas at all.

TON 1542— A negative high-velocity feature is present in the Si III profile at a low level. The wavelength coverage of the spectrum is fairly wide, 1194–1298 Å but the velocity of this possible HVC is badly blended in the Si II λ1260.42 profile by Galactic S II λ1259.52. Thus we are unable to confirm this detection. Since we cannot identify any contaminants at higher redshift responsible for the feature, we accept it as high-velocity Si III detection. However, this detection is at low significance ($\sim 3\sigma$).

TON S180— The data for this target are excellent and cover 1194–1298 Å. There is a strong negative highly-ionized HVC in this sight line thoroughly investigated by CSG05. In the *FUSE* bandpass, the feature was reported as an O VI detection (S03), and it can also be detected in C II λ1036.34 and C III λ977.02. In the STIS spectrum, a corresponding feature is possibly present in Si II λ1260.42, but most of the feature is severely blended with Galactic S II λ1259.52.

VIIZW118— Negative high-velocity absorption is seen in the Si III profile for this sight line. The data quality is fair, but the limited wavelength coverage of 1194–1249 Å prevents the confirmation of this detection. In the *FUSE* bandpass, this was reported as an O VI non-detection (S03). A definite high-velocity feature is seen in C II λ1036.34 over a similar velocity range as the Si III feature. Since there are no known IGM contaminants that could affect the Si III profile, we adopt it as a high-velocity Si III detection.

TABLE 1
High-Velocity Si III Detections from STIS E140M datasets

Sight Line	l (deg)	b (deg)	v_{min} (km s^{-1})	v_{max} (km s^{-1})	W_λ (mÅ)	log$N$(Si III) (N in cm^{-2})
3C 351	90.09	36.38	-221	-150	195±11	> 13.37[a]
			-150	-87	191±9	> 13.40
H 1821+643	94.00	27.41	-165	-75	304±6	> 13.70
HE 0226-4410	253.94	-65.77	119	215	233±14	> 13.27[a]
HS 0624+6907	145.71	23.35	-127	-90	111±7	> 13.06[a]
			105	135	28±7	$12.22^{+0.10}_{-0.13}$
HS 1700+6416	94.40	36.16	-197	-85	378±33	> 13.75
Mrk 279	115.04	46.86	-226	-115	306±7	> 13.55[a]
Mrk 335	108.77	-41.43	-426	-380	41±10	$12.35^{+0.10}_{-0.13}$
			-360	-275	125±14	$12.90^{+0.05}_{-0.05}$
			-257	-237	25±5	$12.17^{+0.09}_{-0.11}$
			-132	-80	137±9	> 13.20
Mrk 509	35.97	-29.86	-338	-256	191±12	> 13.28[a]
			-256	-213	48±8	$12.45^{+0.07}_{-0.08}$
			100	147	80±14	$12.74^{+0.08}_{-0.11}$
Mrk 876	98.27	40.38	-210	-155	178±6	> 13.37
			-155	-100	212±6	> 13.56
NGC 1705	261.08	-38.74	100	148	55±6	$12.52^{+0.05}_{-0.06}$
			220	367	322±13	> 13.56[a]
NGC 3516	133.24	42.40	-187	-115	162±18	> 13.13[a]
NGC 3783	287.46	22.95	100	153	113±17	$12.98^{+0.07}_{-0.09}$
			153	203	63±3	$12.58^{+0.02}_{-0.02}$
			203	288	117±4	$12.87^{+0.01}_{-0.01}$
NGC 4593	297.48	57.40	88	118	43±6	$12.43^{+0.06}_{-0.08}$
			258	291	36±7	$12.33^{+0.08}_{-0.10}$
NGC 7469	83.10	-45.47	-410	-270	405±27	> 13.70
			-270	-237	70±9	> 12.71[a]
			-190	-114	83±19	> 12.68[a]
PG 0953+414	179.79	51.71	-171	-130	64±6	$12.63^{+0.04}_{-0.04}$
			-130	-100	78±20	> 12.99[a]
			85	165	101±9	$12.79^{+0.03}_{-0.04}$
			165	194	20±5	$12.05^{+0.09}_{-0.11}$
PG 1116+215	223.36	68.21	90	125	63±4	$12.66^{+0.03}_{-0.03}$
			130	220	211±7	> 13.36[a]
PG 1211+143	267.55	74.32	160	208	49±4	$12.45^{+0.03}_{-0.03}$
			265	293	22±3	$12.08^{+0.05}_{-0.06}$
PG 1216+069	281.07	68.14	165	234	110±14	$12.87^{+0.05}_{-0.06}$
			234	302	134±13	> 13.08[a]
PG 1259+593	120.56	58.05	-180	-105	184±7	> 13.39[a]
PG 1444+407	69.90	62.72	-164	-109	65±11	$12.57^{+0.07}_{-0.08}$
PHL 1811	47.48	-44.82	-385	-328	46±6	$12.44^{+0.05}_{-0.05}$
			-309	-237	138±6	> 13.03[a]
			-237	-180	187±5	> 13.31
			-180	-128	124±5	> 13.20
PKS 0312-770	293.44	-37.55	70	280	673±30	> 13.96
			280	372	235±15	> 13.39[a]
PKS 0405-123	204.93	-41.76	100	161	43±10	$12.39^{+0.08}_{-0.10}$
PKS 2155-304	17.73	-52.25	-309	-215	34±8	$12.25^{+0.09}_{-0.11}$
			-195	-91	170±8	> 13.16[a]
Q 1230+0115	291.26	63.66	95	152	54±8	$12.55^{+0.05}_{-0.07}$
			285	318	49±5	$12.51^{+0.05}_{-0.05}$
TON 28	200.09	53.21	97	183	89±18	$12.71^{+0.07}_{-0.10}$
TON S210	224.98	-83.16	-266	-221	74±8	> 12.78[a]
			-221	-148	205±10	> 13.41
UGC 12163	92.14	-25.34	-477	-381	293±30	> 13.54
			-372	-324	104±19	> 12.88[a]
			-172	-135	69±16	> 12.72[a]

[a] Although not apparent from the binned data presented in Figure 1, saturation is present in the unbinned data for this sight line. The measured column density is thus taken as a lower limit.

TABLE 2
High-Velocity Si III Detections from STIS G140M datasets

Sight Line	l (deg)	b (deg)	v_{min} (km s^{-1})	v_{max} (km s^{-1})	W_λ (mÅ)	log$N$(Si III) (N in cm^{-2})
ES 438-G009	277.55	29.36	65	168	294±40	> 13.45[a]
			168	268	123±46	$12.87^{+0.14}_{-0.19}$
HE 0340-2703	222.68	-52.13	275	302	55±8	$12.57^{+0.07}_{-0.09}$
HE 1029-1401	259.34	36.52	92	178	243±6	$13.34^{+0.01}_{-0.01}$
			178	263	130±7	$12.91^{+0.02}_{-0.03}$
HS 1543+5921	92.40	46.36	-189	-109	88±32	$12.72^{+0.13}_{-0.20}$
IRAS 08339+6517	150.46	35.60	-273	-100	335±57	$13.37^{+0.06}_{-0.08}$
MCG 10.16.111	144.22	55.08	-235	-100	221±18	$13.29^{+0.05}_{-0.06}$
MRC 2251-178	46.20	-61.33	-324	-179	145±13	$12.94^{+0.03}_{-0.04}$
			100	154	54±10	$12.50^{+0.08}_{-0.12}$
Mrk 110	165.01	44.36	-177	-100	196±24	> 13.20[a]
Mrk 478	59.24	65.04	-158	-100	35±8	$12.27^{+0.09}_{-0.11}$
Mrk 926	64.09	-58.76	-329	-130	221±61	$13.10^{+0.10}_{-0.13}$
Mrk 1044	179.70	-60.48	-252	-160	79±17	$12.63^{+0.08}_{-0.11}$
Mrk 1513	63.67	-29.07	-340	-241	97±11	$12.74^{+0.04}_{-0.05}$
			-241	-160	60±9	$12.51^{+0.06}_{-0.07}$
			-160	-109	23±7	$12.06^{+0.11}_{-0.15}$
NGC 985	180.84	-59.49	-262	-175	51±10	$12.42^{+0.08}_{-0.09}$
			-175	-120	29±7	$12.18^{+0.10}_{-0.12}$
PG 0804+761	138.28	31.03	-176	-80	143±16	$12.99^{+0.06}_{-0.07}$
PG 1049-005	252.28	49.88	85	205	369±39	> 13.55[a]
			205	276	117±30	$12.89^{+0.10}_{-0.13}$
PG 1351+640	111.89	52.02	-213	-100	341±11	> 13.70
PKS 1004+130	225.12	49.12	125	357	334±52	> 13.36[a]
PKS 1103-006	256.66	52.30	115	295	506±84	> 13.72
PKS 2005-489	350.37	-32.60	100	232	156±15	$13.01^{+0.06}_{-0.07}$
Q 1831+731	104.04	27.40	-202	-100	141±17	$13.02^{+0.04}_{-0.05}$
RXSJ 01004-511	299.49	-65.84	100	160	159±16	$13.10^{+0.05}_{-0.05}$
			160	257	148±14	$12.98^{+0.04}_{-0.04}$
TON 730	28.71	78.15	-140	-100	33±11	$12.26^{+0.12}_{-0.17}$
TON 1542	269.44	81.74	-180	-100	37±12	$12.28^{+0.12}_{-0.17}$
TON S180	139.00	-85.07	-232	-70	289±10	$13.29^{+0.02}_{-0.01}$
VIIZW118	151.36	25.99	-189	-100	81±15	$12.66^{+0.07}_{-0.08}$

[a] Although not apparent from the data presented in Figure 2, unresolved saturation is likely present based on the analysis method discussed in § 3. The measured column density is thus taken as a lower limit.

TABLE 3
Sight Lines With No Detected High-Velocity Si III

Sight Line	l (deg)	b (deg)	Velocity Range (km s^{-1})	W_λ (mÅ)	log$N$(Si III) (N in cm^{-2})
3C 273	289.95	64.36	105 to 240	< 16	< 11.89
Mrk 1383	349.22	55.13	100 to200	< 38	< 12.26
NGC 4051	148.89	70.09	-250 to -150	< 62	< 12.49
NGC 5548	31.96	70.50	-150 to -100	< 36	< 12.24
PKS 1302-102	308.59	52.16	220 to 340	< 60	< 12.46

Note. — Upper limits (3σ) over stated velocity range, using E140M echelle data toward 5 sight lines with no high-velocity Si III.

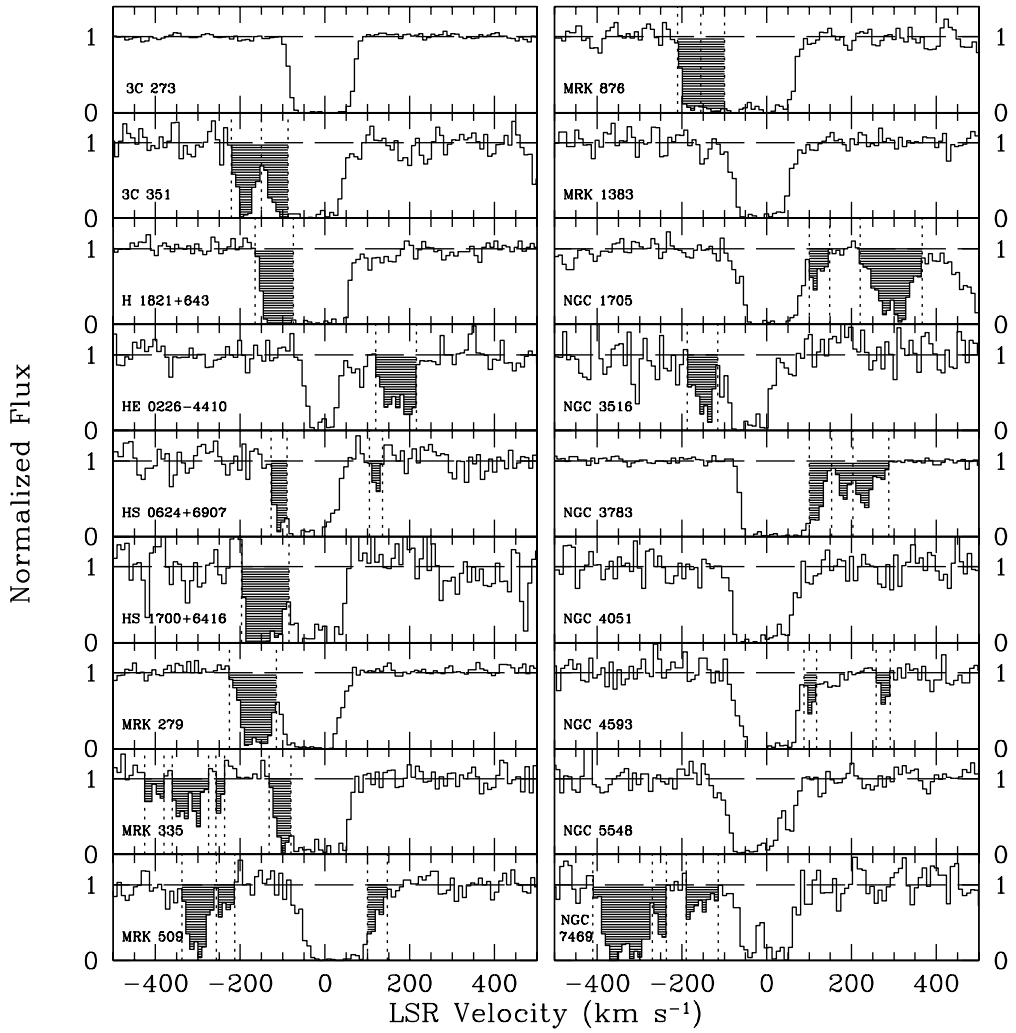

Fig. 1.— Normalized profiles of the Si III λ1206.50 line for 33 sight lines observed with the STIS/E140M echelle. Dashed lines indicate velocity extent of detected HVC components; HVC absorption has been shaded.

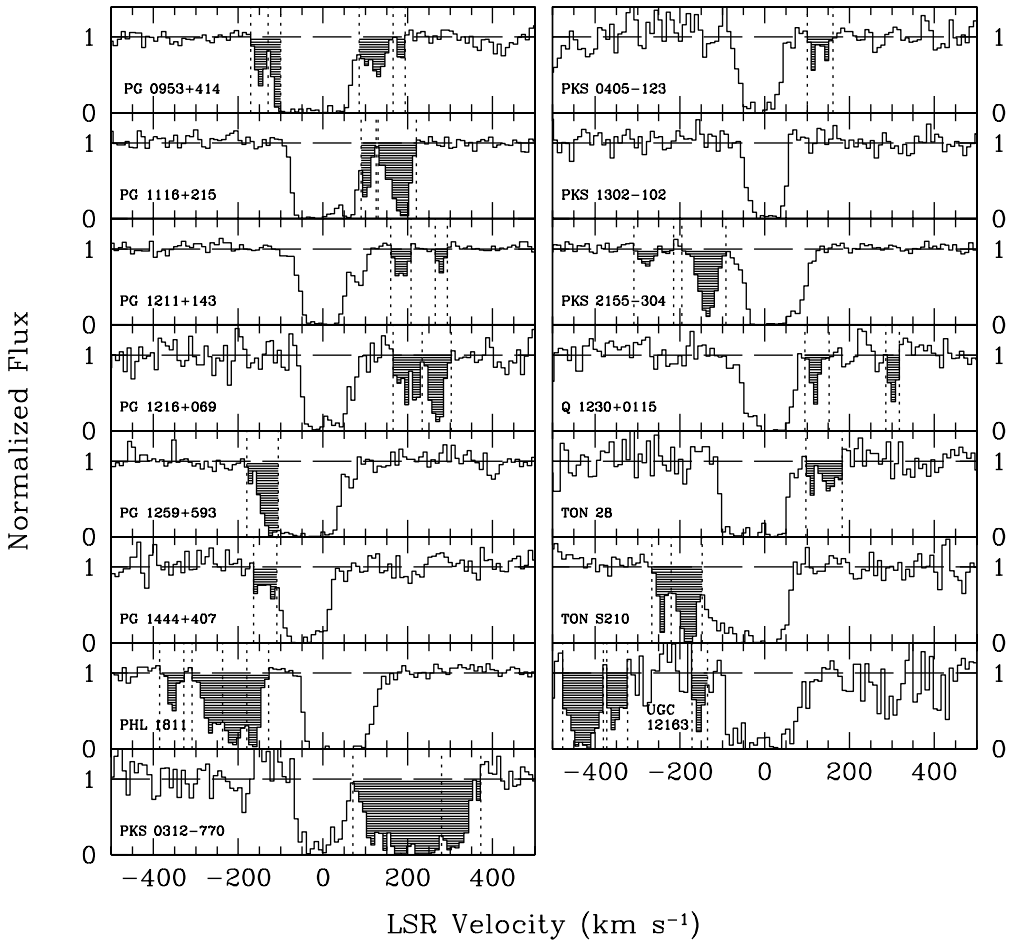

FIG. 1.— Normalized profiles of the Si III λ1206.50 line for 33 sight lines observed with the STIS/E140M echelle.

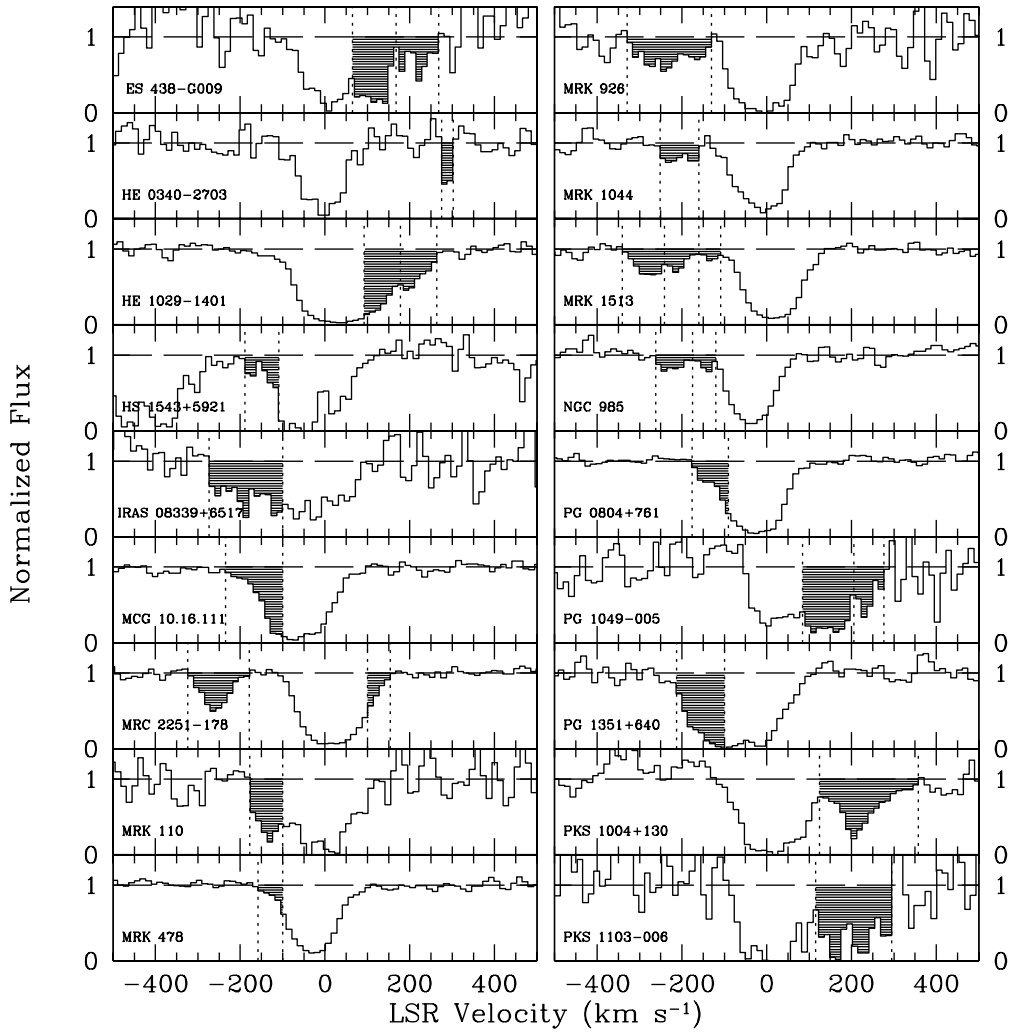

FIG. 2.— Same as Figure 1. Normalized profiles of the Si III λ1206.50 line for 25 sight lines observed with the STIS/G140M grating.

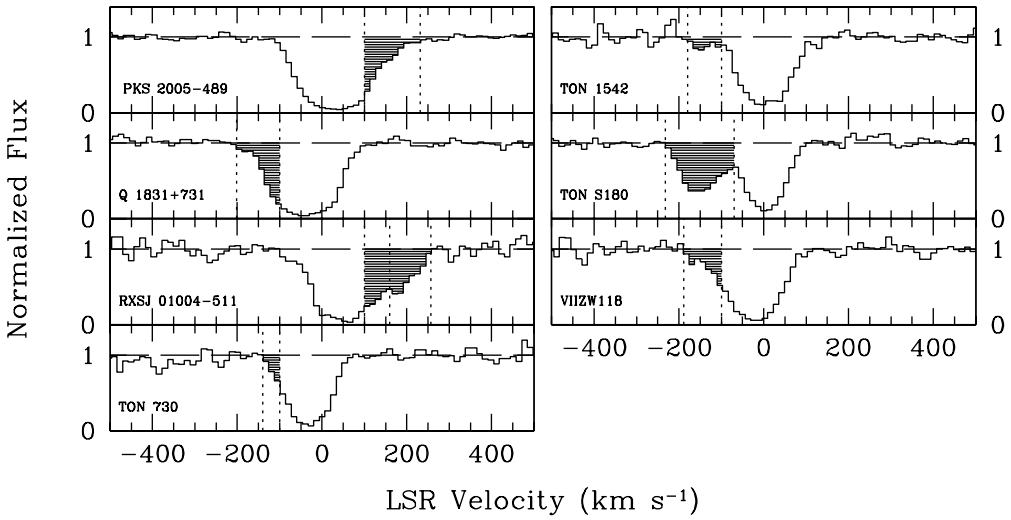

FIG. 2.— Normalized profiles of the Si III λ1206.50 line for 25 sight lines observed with the STIS/G140M grating.

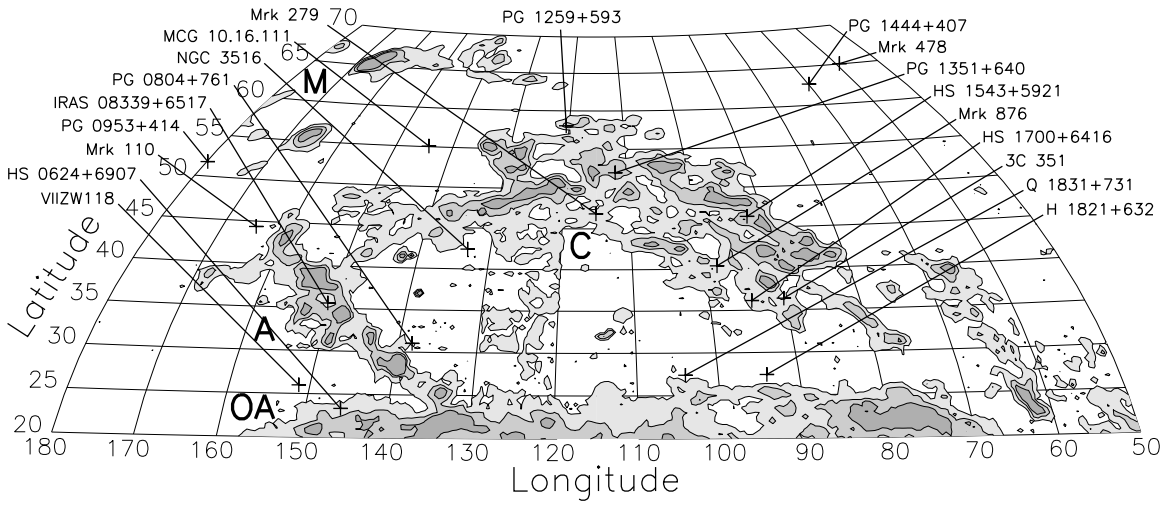

FIG. 3.— Contours of H I column density from the LDS (Hartmann & Burton 1997) for high-velocity gas (-210 km s$^{-1}\leq V_{\rm LSR} \leq -90$ km s^{-1}) in the region $180^\circ \geq l \geq 50^\circ$ and $70^\circ \geq b \geq 20^\circ$. Contour levels are $N_{\rm HI} = 1$, 3, and 6×10^{19} cm^{-2}. The locations of the 19 sight lines in this region are labelled. High-velocity Si III absorption is detected within the plotted velocity range for all 19 sight lines.

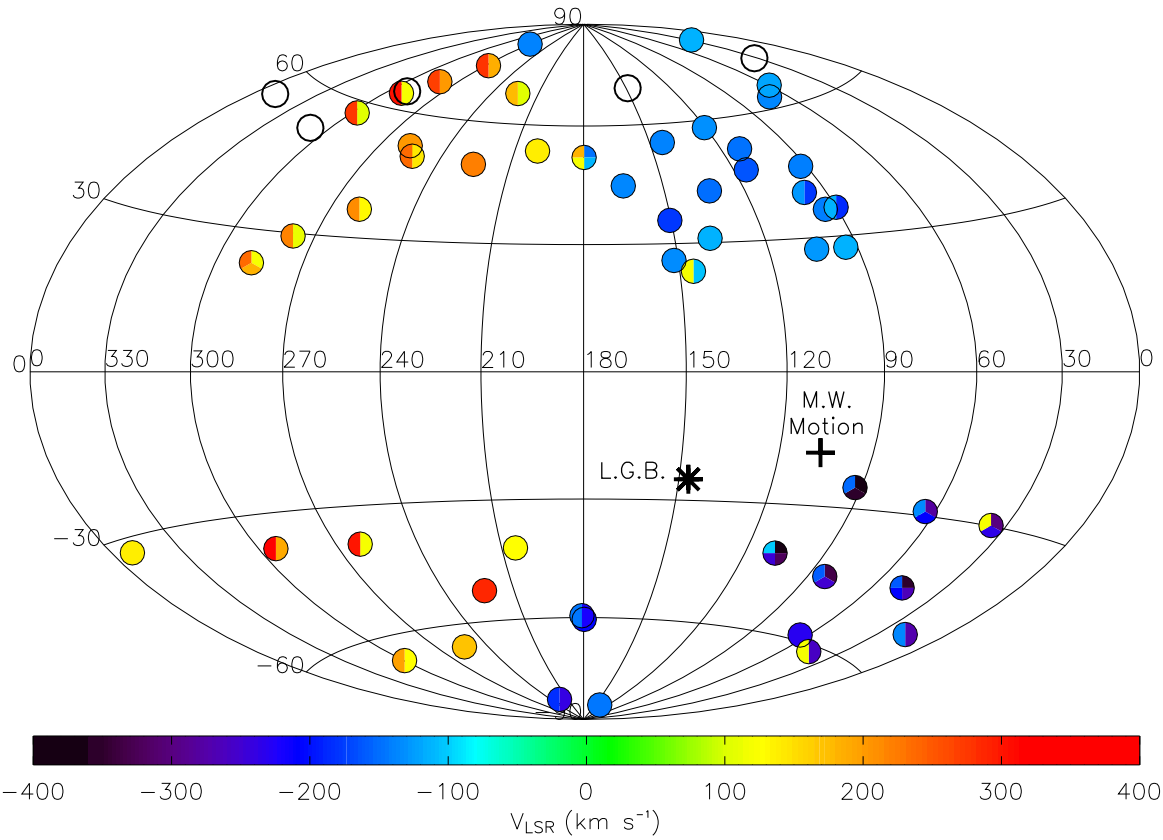

FIG. 4.— All-sky Hammer-Aitoff projection in Galactic coordinates of the locations of the 58 QSO sight lines analyzed for this study. The color scale indicates the velocity centroid of the Si III line for the HVC component(s) in the sight line. For sight lines with multiple HVC components, the circle is split into several colors representing the velocity centroid of each component. Empty circles indicate sight lines where no high-velocity Si III is detected. We mark the Local Group barycenter ($\ell = 147°$, $b = -25°$; Karachentsev & Makarov 1996) by an asterisk, and note with a plus sign the direction of the Milky Way motion ($V = 90$ km s^{-1}, $\ell = 107°$, $b = -18°$; Einasto & Lynden-Bell 1982) with respect to the Local Group barycenter.

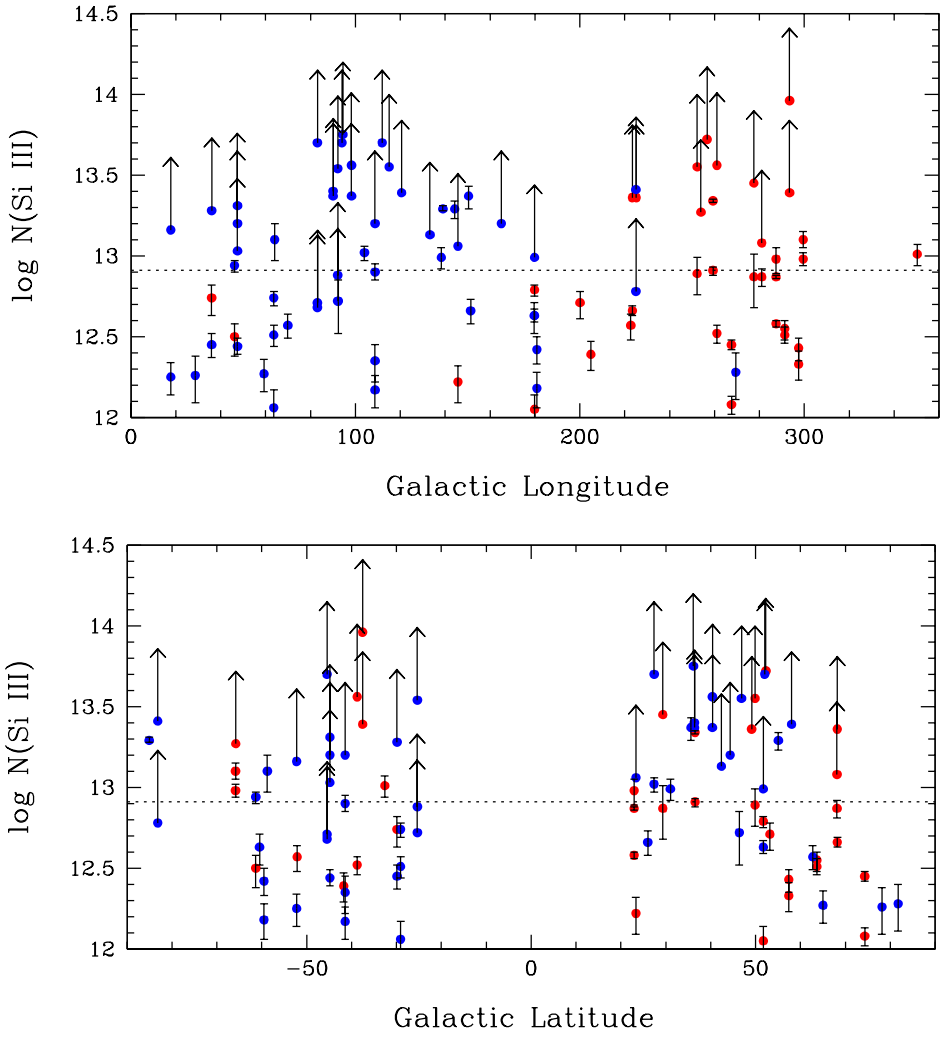

FIG. 5.— Column densities N(cm^{-2}) of Si III vs. Galactic longitude and latitude. Each point represents an individual velocity component for the HVCs. The dashed line represents the median logarithmic Si III column density of 12.91. Lower limits reflect saturation in the strong Si III λ1206.5 absorption line. Red-shifted and blue-shifted components are shown in appropriate colors. No clear trends are apparent, other than possible peaks in Si III (lower limits in column density) around $\ell = 80° - 120°$ and $\ell = 260° - 300°$.

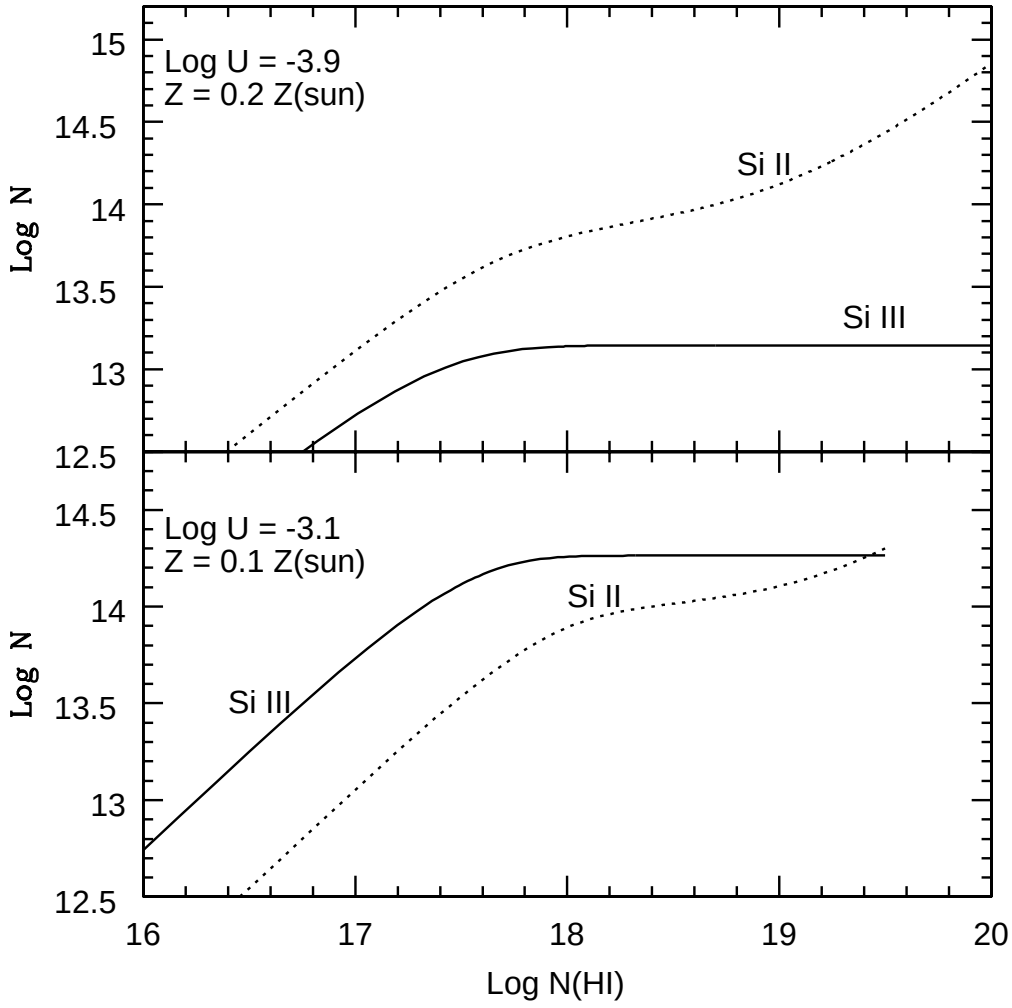

FIG. 6.— Typical HVC photoionization models of Si II and Si III column densities vs. depth into absorber as measured by N_{HI}. Two panels show models with different metallicities and ionization parameters (a) $\log U = -3.9$, $n_H = 0.1$ cm^{-3}, and 20% solar abundances; (b) $\log U = -3.1$, $n_H = 0.016$ cm^{-3}, and 10% solar abundances. These models are similar to those in Shull et al. (2009) and suggest that some ionized HVCs with $N_{SiIII} \geq 10^{13.5}$ cm^{-2} could be detectable in 21-cm emission if log $N_{HI} \geq 17.5$.